Earth-Science Reviews 218 (2021) 103644

Contents lists available at ScienceDirect

Earth-Science Reviews

journal homepage: www.elsevier.com/locate/earscirev

# The importance of tangential motion in the Central Alps: Kinematic analysis and Rb—Sr dating of mylonitic rocks from the Pennine nappes in the eastern Central Alps

Uwe Ring [a,*], Johannes Glodny [b]

[a] Department of Geological Sciences, Stockholm University, 10691 Stockholm, Sweden
[b] GFZ German Research Centre for Geosciences, 14473 Potsdam, Germany

ARTICLE INFO

*Keywords:*
Kinematic analysis
Normal faulting
Out-of-plane deformation
P-T conditions
Rb-Sr geochronology
Central Alps

ABSTRACT

We discuss the important role of tangential stretching in the Central Alps highlighting that the Alps are a truly three-dimensional orogen. A review of pressure-temperature (P-T) conditions allows us to define three major breaks in metamorphic pressure (P-breaks) across the nappe pile. We constrain the kinematics of mylonites associated with these P-breaks and report eight new Rb—Sr multi-mineral isochrons that define the age of the mylonites. Kinematic data and Rb—Sr geochronology indicate that the timing of top-SE normal shearing in the Avers-Turba mylonite zone (≥45–34 Ma; P-break1) and in a zone of distributed top-E normal shearing (>35–30 Ma) above the (ultra)high-P Adula nappe of the distal, thinned European margin (P-breaks 2 and 3). The ages from both sets of mylonite are grading into each other at about 35–34 Ma. All ages appear to postdate high-P metamorphism in the Pennine nappes but are, in part, coeval with and predate (ultra)high-P metamorphism in the underlying Adula nappe of the distal European (Helvetic) margin. The oldest Rb—Sr age of 42.3 ± 2.5 Ma (2σ uncertainties) dates the waning stage of mylonitization and indicates that the Avers-Turba mylonite zone started to operate ≥45 Ma, and predated the exhumation of the Adula nappe by ~10 Ma. We suggest that the motion in the Avers-Turba mylonite zone overlapped with backfolding of the Schams nappe in an extrusion wedge. When this process started, the Adula nappe was still being underthrust/underplated. The ages for distributed top-E normal shearing are contemporaneous with thrusting of the Adula nappe on top of distinctly lower-P Helvetic nappes. When the Adula nappe was being thrust onto non-high-P nappes the necessary reduction of its overburden was largely accomplished by distributed top-E normal faulting above the Adula nappe, and possibly still ongoing top-SE normal shearing. We discuss that major normal shearing occurred during lithospheric shortening. Our data indicate considerable tangential (out-of-plane) movements during overall top-N/NW thrust propagation in the Central Alps and have implications for current tectonic models of the Alps.

## 1. Introduction

The Alps are a classic and well-studied mountain chain known for remarkable along-strike changes in orogenic history, structural style, metamorphism and sedimentation patterns (Fig. 1). Nappe movements during lithospheric shortening range from E-W to N-S (Choukroune et al., 1986; Ratschbacher, 1986; Ring et al., 1988; Schmid and Hass, 1989) and there is also a significant component of orogen-parallel (tangential) extension, especially in the Eastern Alps, since about 30–25 Ma (Steck, 1984; Ratschbacher et al., 1991; Glodny et al., 2008a; Favaro et al., 2015). However, large-scale tectonic models for the Central Alps are essentially restricted to in-plane deformation, highlighting the dominance of top-to-the-N/NW foreland-directed nappe stacking (e.g., Schmid et al., 1996; Schmid et al., 2004; Rosenberg and Kissling, 2013).

The tectonic model of Schmid et al. (1996) still appears to be the 'state-of-the-art' tectonic interpretation of the Tertiary evolution and architecture of the Central Alps. This model used geophysical data and paleogeographic reconstructions to argue that domains located originally to the S/SE were the first to be accreted into the orogenic wedge and that progressive accretion was by sustained top-NW/N thrusting. A key element of the tectonic model is the 32–30 Ma Bergell intrusion, which cuts nappe boundaries in the southeastern Central Alps and serves as an important time marker. The Schmid et al. model is a two-

* Corresponding author.
*E-mail address:* uwe.ring@geo.su.se (U. Ring).

https://doi.org/10.1016/j.earscirev.2021.103644
Received 3 December 2020; Received in revised form 14 February 2021; Accepted 18 April 2021
Available online 23 April 2021

dimensional model that largely neglects any tangential (out-of-plane) motion.

Rosenberg and Kissling (2013) compared three lithospheric-scale cross section across the Central and western Eastern Alps and concluded that the accommodation of Tertiary collisional shortening in the Central Alps varies dramatically along strike. In the Engadine window section (Fig. 1), ~80% of orogenic shortening is concentrated in the overriding (Adriatic) plate. In the Bergell section, shortening is almost equally distributed between overriding and underthrust (European) plate, and in the Simplon section 80% of shortening is accommodated in the underthrusting plate. Rosenberg and Kissling (2013) proposed that these changes are due to pronounced along-strike variations in deep crustal rheology. While this conclusion appears novel and sound, the restoration of the three cross sections also neglects any tangential movement.

While the tectonic models of Schmid et al. (1996) and Rosenberg and Kissling (2013) focus on the Tertiary history of the Central Alps, Winkler (1988) argued that subduction in the eastern Central Alps possibly started already in the early Cretaceous. Based on work by Laubscher (1988), Carminati and Doglioni (2012) suggested that frontal subduction in the Cretaceous has been concentrated in the Western Alps along an *E*-dipping subduction zone. The E-W striking Central and Eastern Alps are considered a right-lateral transpressive part of the Cretaceous/early Cenozoic Alpine orogen (Ring, 1994a; Carminati and Doglioni, 2012). Such a scenario is in line with sedimentation in the Rhenodanubian flysch basin (Fig. 1), which shows a close proximity of source and sink for more than 50 Ma suggesting a strike-slip margin (Hesse, 1981; Waibel and Frisch, 1989). The movement direction of the overriding Adriatic Plate changed in the early Cenozoic (Ring et al., 1988; Platt et al., 1989; Dewey et al., 1989) and caused more orthogonal N/NE-S/SW convergence in the Central Alps.

While there is ample evidence for pronounced foreland-directed thrusting, Price et al. (2018) noted that the large-scale tectonic models do "indicate very little enthusiasm … for large amounts of top-south motion of the Austroalpine allochthon relative to the Pennine zone" in the eastern Central Alps. There, the nappes form an E-dipping stack ranging from structurally deep Helvetic units of the European margin, including the (ultra)high-pressure (P) Adula nappe, up to low-grade Austroalpine nappes and are a key area straddling the Pennine-Austroalpine boundary zone. The study of Price et al. (2018) produced and compiled >350 low-temperature thermochronologic (low-T thermochron) ages and marks a major recent breakthrough in better understanding the tectonic evolution of the Central Alps. Furthermore, Price et al. (2018) analyzed five geologically based models, two of which indicate ~20 km of top-S motion between 40 and 30 Ma and one presents approximately 70 km of top-S motion between 40 and 20 Ma. In addition, the numerical model by Gerya et al. (2002) predicts ~40 km of top-S motion, and the analoque model of Boutelier et al. (2004) shows nearly 100 km of top-S motion. The structural overlap between nappes with contrasting thermal histories at the Austroalpine-Pennine transition is about 70 km from N to S and demand pronounced top-S/SE normal shearing (Price et al., 2018). An estimate of 70 km is in agreement with a structurally derived estimate of 68 km by Weh (1998). Price et al. also noted that the net motion probably also had a large (but not quantified) tangential top-E component. Furthermore, Price et al. (2018) showed that crosscutting relations of the 32–30 Ma-old Bergell intrusion are, at least in part, misleading as contrasting thermal histories between the Pennine and Austroalpine domains require emplacement of the Pennine nappes after 30 Ma.

An interesting feature of the eastern Central Alps are distinct breaks in pressure-temperature (P-T) conditions across the nappe pile (Ring, 1992a; Baudin and Marquer, 1993) (Figs. 2, 3), indicating that large sections of crust are missing within the Pennine nappe pile, especially across the deeper Pennine and Helvetic nappes distinctly below the Pennine-Austroalpine boundary zone. So far it appears that a general conclusion of previous work is that the break from high-P to low-P rocks is located at or near the Pennine-Austroalpine boundary. Another important question is how these P-T breaks relate to pronounced top-S

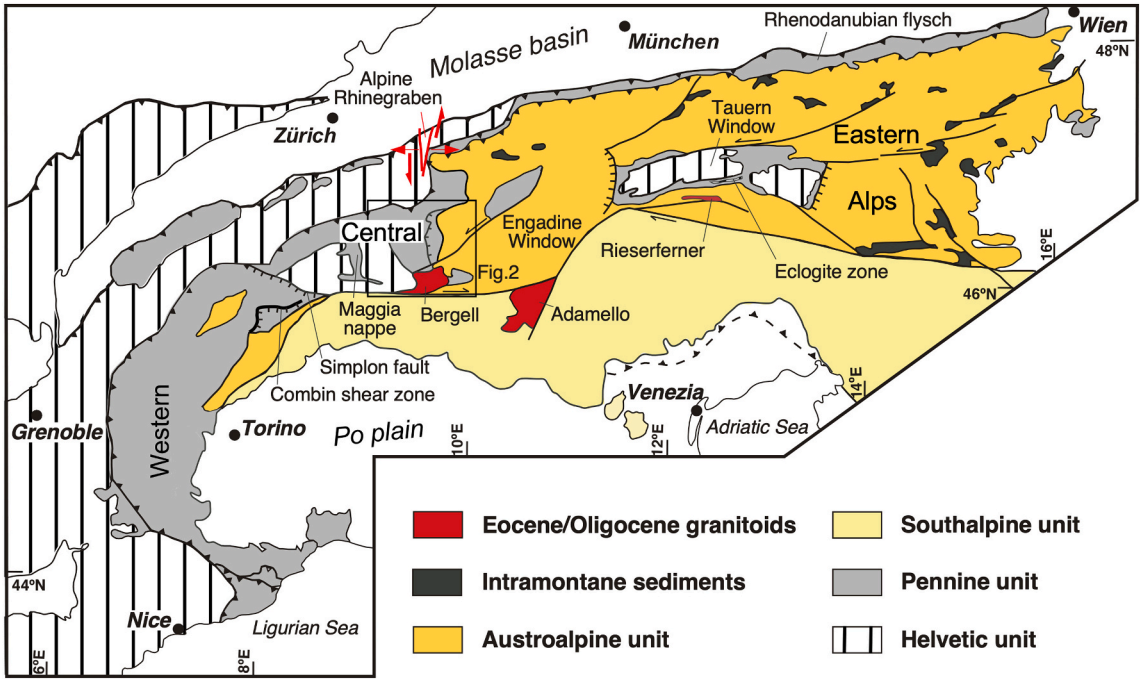


**Fig. 1.** Tectonic overview map of Alps showing Western, Central and Eastern Alps. The main orogenic imprint of the Austroalpine occurred in the Cretaceous, whereas the Central and Western Alps have a strong Tertiary orogenic history. Note the extensional sedimentary basins in the Austroalpine in the Eastern Alps and the lack of these basins in the Central and Western Alps. The 32–30 Ma Bergell intrusion cuts nappe structures in the southeastern Central Alps; in the Tauern Window of the Eastern Alps very high-pressure metamorphism in the Eclogite zone took place at the same time as the intrusion of the Bergell pluton, and nappe stacking below the Eclogite zone occurred afterwards. Also shown is the Alpine Rhinegraben at the northern edge of the Central Alps and the Rhenodanubian flysch basin. Box outlines the map shown in Fig. 2.

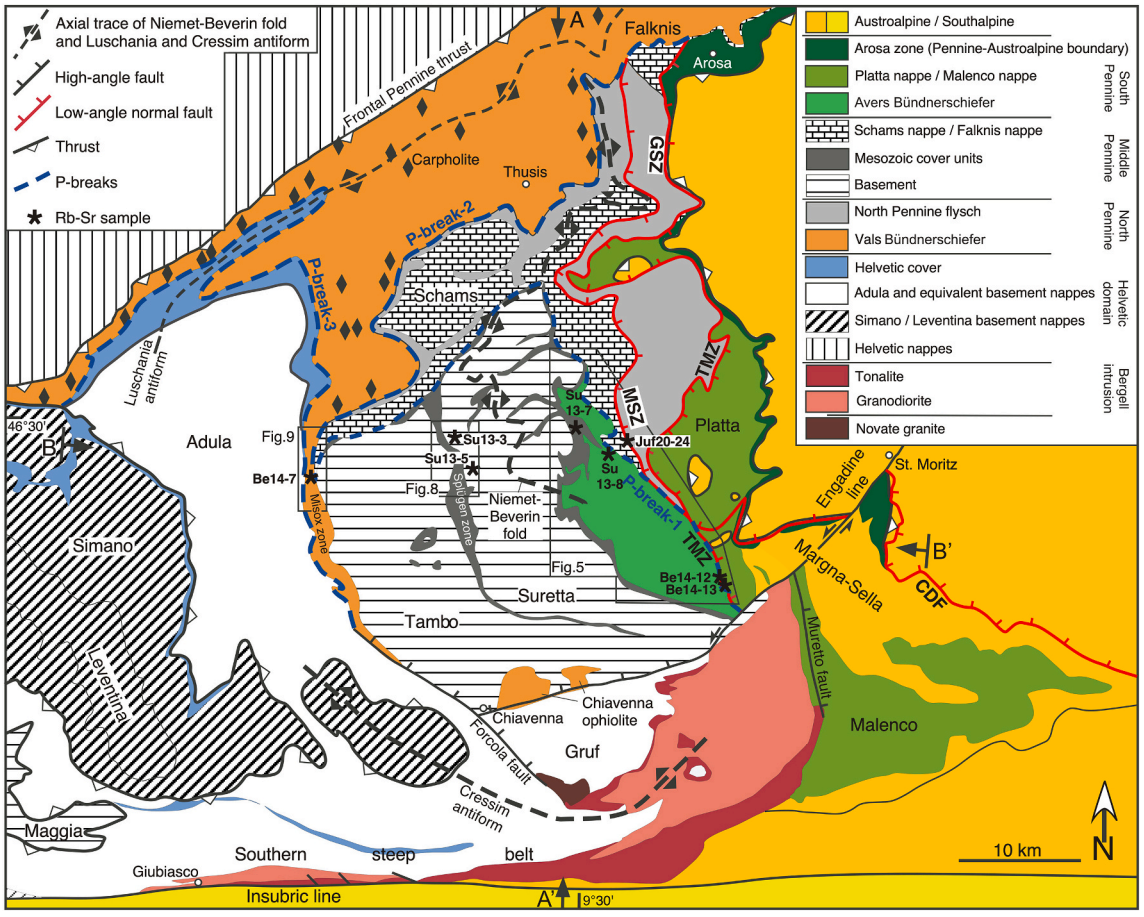


**Fig. 2.** Tectonic map of the eastern Central Alps (modified from Spicher, 1980; Schmid et al., 1996; Price et al., 2018). Shown are major thrusts at the Pennine-Austroalpine boundary, the frontal Pennine thrust and the thrust at the base of the Adula nappe. Also shown are major low-angle normal faults in the vicinity of the Pennine-Austroalpine boundary zone. The Turba mylonite zone (TMZ) is commonly correlated with the Gürgaletsch shear zone (GSZ) (cf., Weh and Froitzheim, 2001). Also shown is the Martegnas shear zone (MSZ). Three major inverse P- breaks are highlighted and numbered 1 to 3 (see text); all surfaces defining the P-breaks converge in the Misox zone. Shown are localities of Rb—Sr samples, the axial traces of the Niemet-Beverin fold, and the Cressim and Luschania antiforms, high-angle normal faults near the Bergell intrusion, the occurrence of carpholite in the Vals Bündnerschiefer according to Oberhänsli et al. (1995) and Wiederkehr et al. (2009) (note that the symbols include pristine carpholite, partially replaced and pseudomorphed carpholite), and cross sections in Fig. 3.

motion (Weh, 1998; Price et al., 2018). Furthermore, there is a well-defined set of mylonitic *E*-trending stretching lineations (Ring, 1992b; Baudin et al., 1993; Marquer et al., 1996) indicating pronounced out-of-plane movements.

The importance of numerical and analoque tectonic models for constraining top-S motion in the Central Alps is mentioned above. Numerical and analoque tectonic models also looked at the exhumation of high-P rocks using the Alps as an example (e.g., Boutelier et al., 2004; Butler et al., 2013). The latter models are two dimensional and thus also strictly cylindrical. (Butler et al., 2013) focused on the Western Alps. The model results support exhumation of the high-P rocks in extrusion wedges (cf., Ring and Glodny, 2010) (note the wedges are called 'plumes' by Butler et al. (2013). The Butler et al. model produced localized orthogonal extension in the upper crust, which is needed in the model to create space for the extruding wedges.

Malusà et al. (2015) critically discussed exhumation models for the Alps and showed differences between the Western and Central Alps due to the obliquity of plate convergence, which was distinctly greater in the Central Alps. The authors suggested that in the Western Alps the upper plate moved slightly away from the trench facilitating exhumation of (ultra)high-P rocks by upper-plate extension. However, the contemplated upper-plate divergence did not take place in the Central Alps (Malusà et al., 2015; their Fig. 8b), which have a distinctly different orogenic strike (Fig. 1).

In this article, we review P-T data and use them in conjunction with deformation structures and their ages to help better understanding the role of top-E and top-S/SE movements in the eastern Central Alps and whether they occurred in a contractional or extensional setting. We conclude that tangential, out-of-plane movements are an important part of the Tertiary orogeny of the Central Alps, which has implications for orogenic-scale models of the Alps.

## 2. Setting

The principal paleogeographic divisons of the Alps are from SE (top) to NW (bottom), the Austroalpine and Southalpine units representing the Adriatic microplate, the tripartite partly oceanic Pennine zone, and the Helvetic nappes of the former European continental margin (Fig. 1) (Argand, 1916; Trümpy, 1960; Frisch, 1979). The Austroalpine nappes contain Permomesozoic cover sequences non-conformably resting on Paleozoic basement. The orogenic development of the Austroalpine largely took place in the Cretaceous and by the latest Cretaceous most of the Austroalpine realm had stabilized into a coherent, relatively undeforming, rigid entity, the 'traineau écraseur' of Argand (1916) or 'orogenic lid' of Laubscher (1983). However, a small part of the Austroalpine was dismembered by Mesozoic lithospheric extension, which created the juxtaposition of a disparate crustal and mantle structural section at the leading edge of the Adriatic passive margin (Schuster

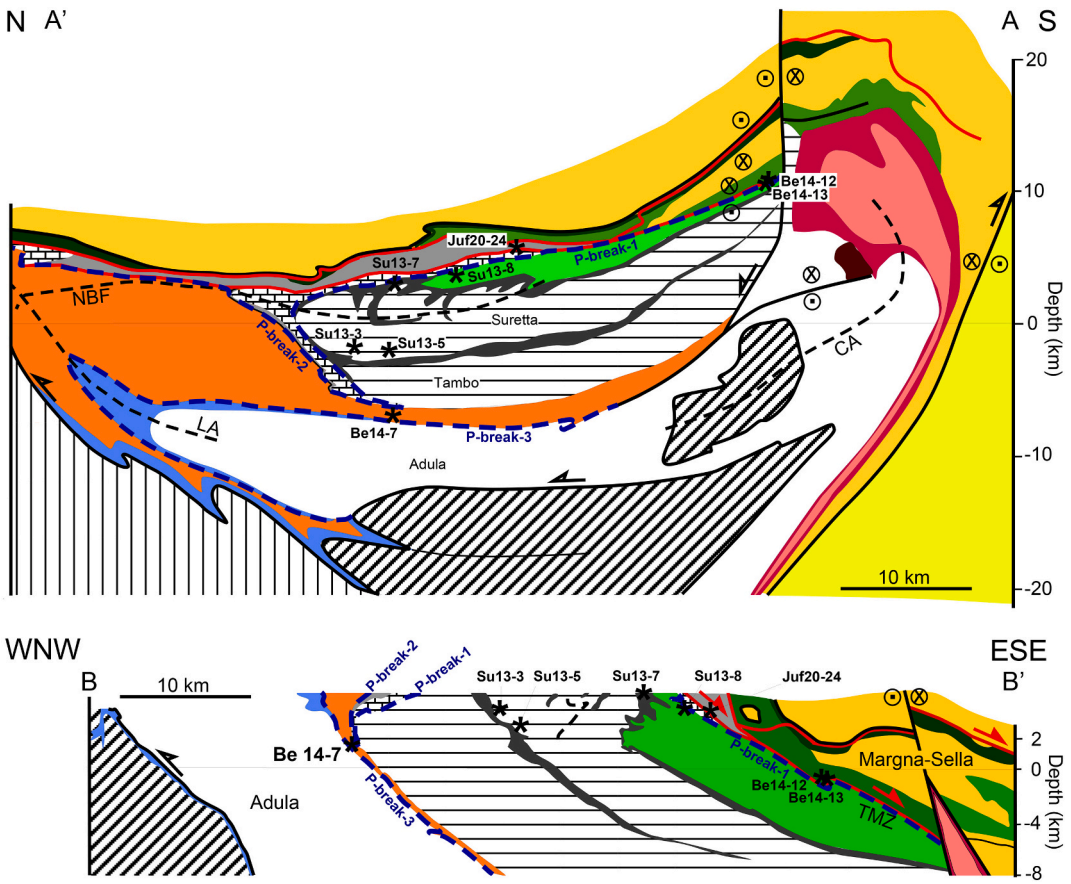


**Fig. 3.** (a) N-S cross section A-A' (modified from Schmid et al., 1990). P-break-1 is folded by the Niemet-Beverin fold and P-break-3 by the Luschania antiform. The strike-slip symbols indicate substantial out-of-plane motion. (b) Schematic WNW-ESE cross section B-B′ showing E/SE-dipping normal fault system near Pennine-Austroalpine boundary and P-breaks. P-break-1 is parallel to the Turba mylonite zone and then cuts down section to the NW.

et al., 2001; Mohn et al., 2011). Of interest here is the Margna-Sella nappe, which formed along this continent-ocean transition and now occupies an intermediate position between the Pennine and Austroalpine domains (Fig. 2) that had not been welded to the 'orogenic lid' by the latest Cretaceous (Price et al., 2018; Ioannidi et al., 2020). The Margna-Sella nappe (Fig. 2) can be regarded as part of the wider Pennine-Austroalpine boundary zone.

The Pennine realm is the most heterogenous paleogeographic domain in the Alps. It consists of the remnants of the Liguria-Piemonte ocean (South Pennine unit), underlain by nappes derived from the Briançonnais microcontinent (Middle Pennine unit), and vestiges of the Valais ocean (North Pennine unit) at the bottom (Trümpy, 1980). The boundary between the Austroalpine and Pennine domains is made up by the Arosa zone, a mélange unit comprising imbricated slices of Austroalpine, South, and rarely Middle Pennine affinity within a matrix composed of South Pennine rocks (Biehler, 1990; Ring et al., 1990; Dürr, 1992). We follow Ring et al. (1990) and Frisch et al. (1994) and regard this mélange unit as the Pennine-Austroalpine boundary zone sensu stricto, and distinguish it from the underlying South Pennine Platta nappe, which is almost entirely made up by rocks derived from the South Pennine ocean (Dietrich, 1970; Dürr, 1992). Below the Platta nappe follow the Avers Bündnerschiefer, which are a vast sequence of calcschist with intercalated serpentinite, metagabbro, metabasalt and marble. The rocks of the Avers Bündnerschiefer represent remnants of the Liguria-Piemonte oceanic lithosphere and mainly its sedimentary cover.

The continental Briançonnais domain is composed of Paleozoic basement (Suretta, Tambo and Maggia nappes), with its late Paleozoic to Mesozoic cover, as well as detached Mesozoic to Eocene cover nappes (Schams and Falknis nappes in Fig. 2). The cover of the basement nappes contains Permo-Carboniferous clastic sequences, which include rare garnet-chloritoid schist (Staub, 1926; own field observations), and Mesozoic marble (Staub, 1926; Scheiber et al., 2012). The detached Schams and Falknis nappes comprise Mesozoic limestone sequences capped, in part, by late Cretaceous to Eocene pelagic marl (Couches Rouges) (von Seidlitz, 1906). Tertiary marl is restricted to the Falknis nappe (Allemann, 1952).

The North Pennine domain comprises extensive sequences of calcschist (Vals Bündnerschiefer) overlain by Tertiary (until ~52 Ma) North Pennine flysch (Nänny, 1948; Ziegler, 1956; Spicher, 1980; Eiermann, 1988; Steinmann, 1994). The North Pennine basin was floored, at least in part, by oceanic lithosphere (Schmid et al., 1990; Dürr et al., 1993; Steinmann and Stille, 1999), the largest remnant of which is the Chiavenna ophiolite (Fig. 2).

Paleogeographically, all nappes below the oceanic North Pennine domain belong to the former European continental margin (Helvetic realm) (Froitzheim et al., 1996). The Adula nappe represents the most distal and thinned part of the European margin and consists of Paleozoic basement with intercalated peridotite (Jenny et al., 1923). Below follow the Simano and Leventina nappes, which are also made up by Paleozoic basement. The deepest Helvetic nappes are thrust onto the frontal Helvetic margin (Helvetic nappes in Figs. 2, 3).

## 3. Review of previous work: Metamorphism, age data and structure

### 3.1. P-T data and their tectonic significance

We review P-T data from the eastern Central Alps for pointing out major breaks in P-T conditions across the nappe pile (Table 1). In the western Austroalpine nappes, Alpine deformation and metamorphism occurred at $P < 5$ kbar and T between 300 and 400°C (Schuster et al., 2004), defining a thermal field gradient of >17–22°C/km (assuming an average rock density of 2700 kg/m$^3$; we use a thermal field gradient of 12–15°/km for distinguishing between high-P subduction-zone and medium-P/T metamorphism). Syn-metamorphic mylonitization in the Margna-Sella nappe occurred at 6–9 kbar and 350–400°C (Liniger, 1992; Ioannidi et al., 2020), indicating a lower thermal field gradient of 11–18°C/km.

Both the Arosa zone and the Platta nappe show low-grade metamorphism increasing from N (~3 kbar, 250°C) to S (~5 kbar, 350°C) (Trommsdorff and Evans, 1974) defining a thermal field gradient of 19–23°C/km. Low-P metamorphism is suggested by illite b0 values (Guidotti and Sassi, 1986) of 8.989–9.022 Å and vitrinite reflectance data (Ferreiro Mählmann and Giger, 2010). The data of Ferreiro Mählmann and Giger (2010) yielded a thermal and barometric field gradient of 22 ± 2°C/km and 0.3 kbar/km, respectively. A major P-T break occurs within the South Pennine unit between the Platta nappe and the Avers Bündnerschiefer, as the latter record high-P conditions of 12–14 kbar at 380–420°C with a low thermal field gradient of 7–9°C/km (Ring, 1992a).

The Middle Pennine Tambo and Suretta basement nappes also show high-P metamorphism, with 9–12 kbar at ~400°C for the Suretta nappe (Ring, 1992a) and 10–13 kbar and 400–450°C for the Tambo nappe (Baudin and Marquer, 1993; Ring, 1992a). The data imply a thermal field gradient of 9–12°C/km. Engi et al. (2004) argued that garnet and chloritoid porphyroblasts in the Permo-Carboniferous cover of the Suretta nappe suggest that these estimates reflect minimum conditions. Metamorphic grade in the Schams nappe is considered lower greenschist facies, with temperatures around 300–400°C and no indications for high-P metamorphism (Schreurs, 1993). A non-high-P scenario is supported by the occurrence of stilpnomelane and illite (Schreurs, 1993), as the upper P limit of stilpnomelane is 4 kbar at 440 ± 15°C (Nitsch, 1970). The data from the Schams nappe crudely suggest a thermal field gradient of >20–25°C/km. In the Falknis nappe further N, illite, smectite, glauconite, pyrophyllite and stilpnomelane are indicative of high diagenetic grade and very low-grade metamorphism (Ferreiro Mählmann and Giger, 2010).

The North Pennine Vals Bündnerschiefer experienced high-P metamorphism at 11–14 kbar and 350–400°C (7–10°C/km thermal field gradient) (Bousquet et al., 2002). In the southern Misox zone, the Vals Bündnerschiefer record higher P and T at >12 kbar and ~ 510 ± 50°C (Oberhänsli, 1994), indicating an increase in high-P metamorphic conditions from N to S as already suggested by Nabholz (1945). In contrast, the North Pennine flysch does not show any evidence for high-P metamorphism. Ferreiro-Mählmann (1996) reported clinozoisite, muscovite and stilpnomelane and T of 350–430°C, suggesting a thermal field gradient >23°C/km (see above for maximum P of stilpnomelane). This indicates another major P-T break at the interface between the Vals Bündnerschiefer and the North Pennine flysch (Figs. 2 and 3).

The Adula nappe records a distinct N-S gradient for high-P metamorphism. Older studies report peak P-T conditions of ~10–15 kbar/450–550°C in the northern, 15–25 kbar/550–650°C in the central, and >20 kbar/800°C in the southern Adula nappe (Heinrich, 1986; Meyre et al., 1999). More recent geothermobarometric studies (Dale and Holland, 2003) resulted in higher P-T conditions of ~17 kbar/640°C in the northern, 22 kbar/750°C in the central and 25 kbar/750°C in the southern Adula nappe. Dale and Holland (2003) showed a consistent metamorphic field gradient of 9.6 ± 2.0°C/km and 0.2 ± 0.05 kbar/km

**Table 1**
Compiled ages for mylonitization and cooling, and P-T conditions of early metamorphism with thermal field gradients

| Unit/nappe | Age range (Ma) | P-T of early (high-P) metamorphism and thermal field gradient |
|---|---|---|
| **Austroalpine** | | |
| *Austroalpine nappes above Corvatsch detachment fault (CDF)* | | <5 kbar, 300-400°C[1] 17-22°C/km |
| Ar/Ar mylonite (Err nappe)[1] | 89.1 ± 2.7 – 76.1 ± 2.3 | |
| ZFT[2] | 53.4 ± 8.5 | |
| ZHe[2] | 56.5 ± 9.4 – 37.3 ± 3.2 | |
| *Sella-Marna nappe below CDF* | 63.0 ± 3.0 | 6-9 kbar, 350-400°C[3] |
| U-Pb Rt peak metamorphism[4] | | *11-18°C/km* |
| U-Pb Ttn decompression[4] | 54.7 ± 4.1 | |
| Ar/Ar mylonite[2] | 50.0 ± 0.6 | |
| Rb-Sr mylonite[5] | 48.9 ± 0.6 | |
| ZFT[2] | 74.5 ± 10.2 – 58.0 ± 11.4 | |
| ZHe[2] | 23.6 ± 0.4 – 22.3 ± 0.5 | |
| **Austroalpine-Pennine boundary***(Arosa Zone)* | | 3-5 kbar, 250-350°C[6,7] 19-23°C/km |
| K-Ar metamorphism | 63.4 ± 2.0 – 59.4 ± 14.8 | |
| Rb-Sr mylonite[8] | 53.8 ± 0.6 – 47.1 ± 0.4 | |
| **South Pennine** | | |
| *Malenco* | | 5-6 kbar, 350-400°C[9] |
| Ar/Ar Amph peak metamorphism[9] | 91-67 Ma | 16-22°C/km |
| *Platta* | | 3-5 kbar, 250-350°C[10] |
| Ar/Ar Amph deformation[1] | 72.4 ± 0.9 – 68.2 ± 2.5 | 19-23°C/km |
| ZHe[2] | 48.7 ± 7.2 – 22.8 ± 1.6 | |
| *Avers Bündnerschiefer* | | 12-14 kbar, 380-420°C[11] |
| ZFT[2] | 35.5 ± 11.7 | *7-9°C/km* |
| ZHe[2] | 21.4 ± 0.7 | |
| **Turba mylonite zone** | | |
| Ar/Ar mylonite[2] | 37.7 ± 1.2 | |
| ZFT[2] | 35.5 ± 5.8 | |
| ZHe[2] | 25.7 ± 1.2 – 21.4 ± 0.7 | |
| **Middle Pennine** | | very low-grade metamorphism |
| *Mesozoic cover (Falknis nappe)* ZHe[2] | 44.3 ± 5.4 | |
| *Schams nappe* K-Ar illite | 51.1-30.3 ± 0.7 | 4 kbar, 300-400°C[12] |
| *Basement (Suretta/Tambo)* | | 9-13 kbar, 400-450°C[11, 13] |
| Ar/Ar HP mylonite[14] | 46.0 ± 5.0 | *9-12°C/km* |
| Rb-Sr deformation[15] | 47.4 ± 1.6 – 35.2 ± 2.7 | |
| Ar/Ar top-E mylonite | 35.7 ± 0.6 | |
| ZFT[16] | 22.1 ± 2.8 – 18.1 ± 2.4 | |
| ZHe[2] | 24.5±1.4 – 14.6±0.6 | |
| **North Pennine** | | |
| *HP Bündnerschiefer* | | 11-14 kbar, 350-400°C[17] |
| Ar/Ar HP deformation[18] | 45-37 Ma (41.2 ± 1.2 mean age) | *7-10°C/km* |
| Ar/Ar exhumation[18] | 36-33 (34.2 ± 1.2 mean age) | |
| ZHe[2] (influenced by Lepontine metamorphism) | 8.8 ± 0.8 | |
| *NP flysch* | | <4kbar, 350-430°C[17] |
| ZHe[2] | 29.1 ± 1.1 – 20.4 ± 1.1 | >23°C/km |
| **Distal Helevtic margin** | | |
| *Adula* | | 17-25 kbar, 640-750°C[19] |
| HP metamorphism[20,21,22] (various methods) | 43.9 ± 5.7 – 35.8 ± 1.6 | *8-10°C/km* |

(*continued on next page*)

**Table 1** (*continued*)

| Unit/nappe | Age range (Ma) | P-T of early (high-P) metamorphism and thermal field gradient |
|---|---|---|
| Initial decompression[23] | 34.2 ± 0.2 | |
| Amphibolite-facies metamorphism[24,25,26] | 32.8 ± 0.6 – 31.4 ± 0.5 | |
| ZFT[27] | 17.4 ± 1.8 | |
| ZHe[2] | 12.3 ± 1.2 – 11.7 ± 0.6 | |

Data: [1]Handy et al. (1996), [2] Price et al. (2018), [3]Liniger (1992), [4]Picazo et al. (2019), [5]Ioannidi et al. (2020), [6]Ferreiro-Mählmann (1996), [7]Ring et al. (1989), [8]Bachmann et al. (2009), [9]Villa et al. (2000), [10]Trommsdorff (1983), [11]Ring (1992a), [12]Schreurs (1993), [13]Baudin and Marquer (1993), [14]Challandes et al. (2003), [15]Steinitz and Jäger (1981), [16]Hunziker et al. (1992), [17]Bousquet et al. (2002), [18]Wiederkehr et al. (2009), [19]Dale and Holland (2003), [20]Brouwer et al. (2005), [21]Becker (1993), [22]Herwartz et al. (2011), [23]Hermann et al. (2006), [24]Liati and Gebauer (2003), [25]Rubatto et al. (2009), [26]Nicollet et al. (2018), [27]Gebauer et al. (1992). Thermal field gradient is calculated using average rock density of 2700 kg/m$^3$; values in italics indicate subduction-zone metamorphism (see text for definition). ZFT = zircon fission track, ZHe = zircon (U—Th)/He, Rt = rutile, Ttn = titanite, Amph = amphibole, HP = high-pressure metamorphism, NP = North Pennine.

over the frontal 25 km of the nappe. This field gradient has been used by Price et al. (2018) to restore a coherent 15-km-thick Pennine/distal Helvetic slab from 10 to 80 km depth, which translates into a down-dip length of ~100 km for a 45°-dipping subduction zone. The restoration of Price et al. (2018) predicts that this 'slab' largely remained coherent during subduction and exhumation. During incipient exhumation, Pellegrino et al. (2020) showed for the southern Adula nappe that eclogite-derived melt interacted with garnet peridotite at high-P conditions.

The nappes below the Adula nappe do not show Alpine high-P metamorphism (Ring, 1992a) indicating another profound P-T break. The Simano nappe records P-T conditions of ~12 kbar/580–630°C (Irouschek, 1983) or 9–11 kbar at ~500°C (Rütti, 2003), defining a thermal field gradient of 11–15°C/km. The Leventina nappe records ~8 kbar/~550°C in the north and ~10 kbar/~650°C in the south (thermal field gradient of ~18°C/km) (Rütti et al., 2008).

This summary reveals a number of important P-T breaks across the nappe pile in the eastern Central Alps (Figs. 2, 3). From top to bottom there are three major inverse breaks where lower P rocks rest tectonically above higher P rocks, which in the following we refer to as 'P-breaks' (as T is not changing much): (1) The break between the Platta nappe and the Avers Bündnerschiefer is of the order of 9 kbar (equivalent to about 33 km of crustal section) (P-break-1 in Figs. 2, 3). The thermal field gradient across this P-break changes from <10°C/km to >20°C/km. P-break-1 is wrapping around the frontal Tambo and Suretta nappes and is apparently folded by the Niemet-Beverin fold. (2) The contact between the North Pennine flysch and the Schams/Falknis nappes with the underlying Vals Bündnerschiefer corresponds to another break of about 9 kbar (P-break-2 in Figs. 2, 3), with a similar change in thermal field gradients as across P-break-1. (3) Between the high-P rocks of the Tambo and Adula nappes across the Misox zone, which may be of the order of ~5 kbar (equaling ~19 km) (P-break-3 in Figs. 2, 3). P-break-3 is not associated with any change in the thermal field gradient. Interestingly all three surfaces marking the P-breaks converge in the Misox zone, which compared to the rest of the Vals Bündnerschiefer is a very thin zone. At least P-break-2 cuts up structural section to the N. Because P-break-1 appears to be folded by the Nimet-Beverin fold it is plausible that it roots in the Misox zone. If so, P-break-1 would also cut up structural section from the North Pennine across the Middle Pennine into the South Pennine zone.

There are also forward P-breaks (i.e., higher P on lower P rocks) deep down in the nappe pile. The most pronounced one is between the Adula and Simano nappes corresponding to >10 kbar (equaling >37 km). It appears as if this forward P-break is cutting inverse P-break 3 (Figs. 2, 3). Another break occurs at the frontal Pennine thrust. There is a minor P-break of about 1–2 kbar between the Simano and Leventina nappes. In the remainder of the article, we only consider the pronounced forward P-break underneath the Adula nappe, which associated with a modest increase in the thermal field gradient structurally downwards (Table 1).

### 3.2. Age data

Well-defined isotopic ages for deformation events across the Austroalpine-Pennine boundary zone and the Pennine nappe stack of the eastern Central Alps are scarce. In general, previous data show an age progression (younging of ages) from top to bottom, i.e., from the Austroalpine units into the South, Middle and North Pennine nappes (Table 1). Note that the isotopic age data for deformation and metamorphism reported in Table 1 represent the waning stages of these processes, as the daughter products of the radioactive decay start accumulating in minerals only after they stop reacting and recrystallizing (Villa, 2010, 2016). However, if a number of age data are reported from the same shear zone, the spread in ages might be considered a minimum estimate for the true duration of deformative or metamorphic processes. This is because recrystallization may stop earlier in some segments, while deformation-induced or deformation-facilitating fluid access may still prevail in other segments of a shear zone or a metamorphically reacting body of rock.

In the Austroalpine nappes, deformation and metamorphism occurred in the middle Cretaceous and progressed structurally downwards into the Arosa zone and Platta nappe at about 80–60 Ma (Hunziker et al., 1992; Handy et al., 1996). Picazo et al. (2019) reported a U—Pb rutile age of 63 ± 3 Ma for peak metamorphism in the Margna-Sella nappe. Mylonitization resulting from top-W/SW thrusting (Liniger, 1992) in the Margna-Sella nappe directly above the Austroalpine-Pennine boundary zone sensu stricto, was dated by Price et al. (2018) at 50 ± 0.6 Ma ($^{40}$Ar/$^{39}$Ar white-mica age) and Ioannidi et al. (2020) at 48.9 ± 0.9 Ma (Rb—Sr white-mica-based isochron age). The mylonitization ages are similar to a titanite U—Pb isochron age of 54.7 ± 4.1 Ma for decompression from high-P metamorphism in the Margna-Sella nappe (Picazo et al., 2019). Rb—Sr dating of synkinematic white mica from the Arosa zone constrained the final stages of top-W thrusting along the Austroalpine-Pennine boundary between 53.9 ± 0.6 and 47.1 ± 0.4 Ma (Bachmann et al., 2009). It appears that the consistent ages of about 50 Ma reflect the cessation of deformation at the wider Pennine-Austroalpine boundary zone and are coeval with the termination of sedimentation in the North Pennine flysch at ~52 Ma and the Couches Rouges sediments in the Middle Pennine Falknis nappe.

Price et al. (2018) obtained a $^{40}$Ar/$^{39}$Ar white-mica age of 37.7 ± 1.1 Ma and a zircon fission-track (ZFT) age of 35.5 ± 5.8 Ma from the Turba mylonite zone. For the underlying northern Suretta nappe, Challandes et al. (2003) provided one single $^{40}$Ar/$^{39}$Ar phengite age of 46 ± 5 Ma for mylonitic deformation at high-P metamorphic conditions. This age is similar to K/Ar and Rb—Sr phengites ages of 47.4 ± 1.6 Ma (Steinitz and Jäger, 1981), and 55 ± 1 Ma and 49 ± 1 Ma (Hurford et al., 1989) from the Suretta nappe. Steinitz and Jäger (1981) also reported a Rb—Sr phengite age of 35.2 ± 2.7 Ma from the Suretta nappe.

Schreurs (1993) obtained four K—Ar illite ages of 60.1 ± 1.3 Ma to 30.3 ± 0.7 Ma from the Schams nappe. The data suggest a trend to older ages with increasing grain size. Schreurs (1993) argued that K—Ar ages for the <2 μm grain-size fractions of 45.1–30.3 Ma reflect the first deformation stage in the Schams nappe. The older K—Ar illite ages are interpreted to be incompletely reset attesting to the low-grade, non-high-P metamorphism envisaged for the Schams nappe (Schreurs, 1993).

In the North Pennine flysch, robust upper age constraints for the onset of deformation are early Eocene (~52 Ma) fossils ((Nänny, 1946); Ziegler, 1956; Eiermann, 1988). For the Vals Bündnerschiefer, Wiederkehr et al. (2009) interpreted $^{40}$Ar/$^{39}$Ar ages of 45–37 Ma (41.23 ±

1.22 Ma weighted mean age) of phengite coexisting with Fe—Mg carpholite to reflect deformation at peak high-P conditions. Wiederkehr et al. (2009) further suggested that the replacement of carpholite by white mica during initial exhumation is dated between 36 and 33 Ma (34.2 ± 1.2 mean age) (Table 1).

For high-P metamorphism in the Adula nappe of the extended distal Helvetic margin, Becker (1993) reported garnet-clinopyroxene-based Sm—Nd ages between 43.9 ± 5.7 and 39.1 ± 3.5 Ma, and Gebauer (1996, 1999) U—Pb SHRIMP zircon ages from garnet peridotites and eclogites of 43 and 35 Ma. Brouwer et al. (2005) obtained three garnet-based Lu—Hf ages of 38.1 ± 2.9 Ma, 36.6 ± 8.9 Ma and 35.8 ± 1.6 Ma for the southern Adula nappe, and Herwartz et al. (2011) a Lu—Hf garnet-omphacite-whole rock age of 37.1 ± 0.9 Ma for the northern Adula nappe. Despite their rather large spread, all ages appear to indicate that high-P metamorphism in the Adula nappe is about 43–35 Ma in age (probably <40 Ma). Importantly, Hermann et al. (2006) showed that a U—Pb SHRIMP zircon age of 34.2 ± 0.2 Ma is related to incipient exhumation close to peak high-P conditions in the Adula nappe. This age is indistinguishable from the mean exhumation age of 34.2 ± 1.2 given by Wiederkehr et al. (2009) for the directly overlying Vals Bündnerschiefer. Hermann et al. (2006) interpreted an age of 32.9 ± 0.3 Ma as dating an exhumation stage at ~7 kbar and 700°C, and Rubatto et al. (2009) similar U—Pb SHRIMP zircon ages between 32.8 ± 0.6 Ma and 31.4 ± 0.5 Ma as dating amphibolite-facies metamorphism following the high-P stage. These ages are similar to U—Pb zircon-rim ages of 32.7 ± 0.5 Ma (Liati and Gebauer, 2003) and a weighted mean U—Pb monazite age of 31.8 ± 0.3 Ma (Nicollet et al., 2018) for ultrahigh-T metamorphism (Tumiati et al., 2018) in the Gruf complex, which tectonically is part of the Adula nappe.

The Hermann et al. (2006) ages indicate minimum exhumation rates between 34.2 ± 0.2 and 32.9 ± 0.3 Ma of >15 km/Ma for the southern Adula nappe during thrusting onto the Simano nappe. Thrusting in the frontal Helvetic nappes commenced at 35–30 Ma (Hunziker, 1986; Kirschner et al., 1996; Simon-Labric et al., 2009), which is coeval with thrusting of the Adula nappe onto the Simano nappe and records an important stage of nappe imbrication at the leading edge of the European margin. Amphibolite-facies metamorphism still affected the nappes in the vicinity of the Frontal Pennine thrust (Fig. 2) at ~20–18 Ma (Janots et al., 2009), and migmatization at temperatures of ~650°C occurred in these deep distal European margin nappes close to the Insubric line until ~22 Ma (Rubatto et al., 2009).

Parts of the nappe pile were intruded in the Oligocene by the calc-alkaline Bergell intrusion (Figs. 1, 2). This composite pluton comprises a 31.9 ± 0.1 and 31.5 ± 0.4 Ma old tonalite flanking the main 30 ± 0.2 Ma granodiorite body (von Blanckenburg, 1992; Oberli et al., 2004). The Bergell pluton is strongly dextrally sheared at the Insubric line (Fig. 2). The Novate granite represents the final phase of magmatism at 24 ± 1.2 Ma (Liati et al., 2000). In contrast to the Bergell intrusion, the Novate granite is a S-type leucogranite derived from lower-crustal partial melting (von Blanckenburg, 1992), coeval with the later stages of high-T metamorphism close to the Insubric line.

The onset of rapid erosion of the Bergell pluton occurred at ~25 Ma (Malusà et al., 2011). The average erosion rate between ~25 and 16 Ma was 1.3–1.4 km/Ma for the main body and 2 km/Ma for the western tail of the intrusion (Malusà et al., 2011). Inferred erosion rates since 16 Ma are indistinguishable in the main body and in the western tail and constrain N—S tilting of the pluton to the interval between ~25 and 16 Ma (Garzanti and Malusà, 2008).

The low-T thermochron ages of Price et al. (2018) (Table 1) constrain the shallow exhumation history of the nappes of the eastern Central

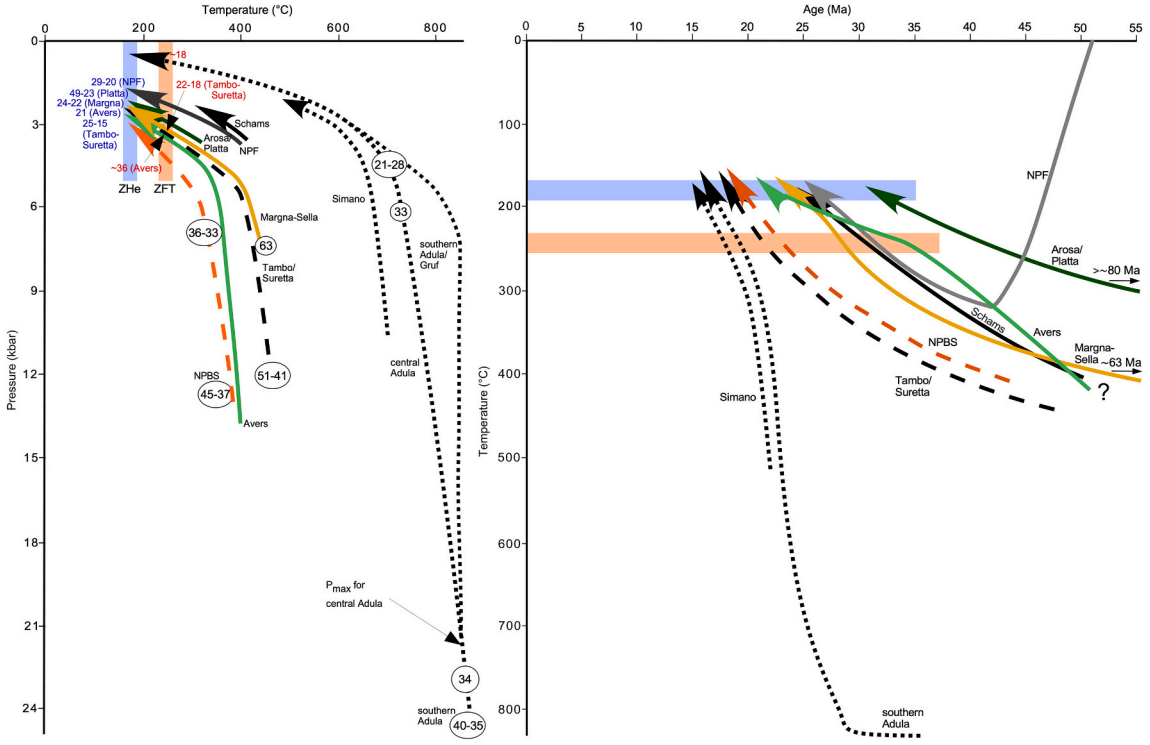


**Fig. 4.** (a) P-T paths for various nappes in the eastern Central Alps based on ages for high-P metamorphism and exhumation as discussed in text. Note that the Adula nappe shows by far the highest P-T conditions (note that we show separate P-T paths for the southern and central Adula nappe), the Avers (South Pennine) and Vals (North Pennine) Bündnerschiefer (NPBS), as well as the Middle Pennine Tambo/Suretta basement nappes show largely similar P-T conditions, and the Schams and Arosa/Platta units, as well as the North Pennine flysch (NPF) lack a high-P overprint marking severe P-breaks with other units. The Austroalpine Margna-Sella nappe occupies an intermediate position in P-T space. (b) T-t path showing that upper units (Arosa/Platta, Schams, Margna-Sella, North Pennine flysch, and also Avers Bündnerschiefer) cooled earlier than the Suretta/Tambo nappes and the Vals Bündnerschiefer. The Adula nappe shows a unique T-t history and remains hot until about 20 Ma. Zircon fission-track (ZFT) and (U—Th)/He zircon (ZHe) ages according to Price et al. (2018); refer to Figs. 2 and 3 for relating P-breaks to the structure of the nappe pile and Table 1 for data.

Alps. Their data define three distinct nappe packages (Fig. 4): (1) the upper nappes (Margna-Sella, Arosa/Platta, Avers, Schams and North Pennine flysch) which cooled through 240–180°C (closure T used by Price et al. (2018) for ZFT and ZHe ((U—Th)/He in zircon) in and before the Oligocene (in part the ZFT ages are close in time to the ages for their maximum burial) (solid lines in Fig. 4b). (2) The Tambo/Suretta nappes and the Vals Bündnerschiefer appear to occupy an intermediate position (dashed lines in Fig. 4b) with early Miocene ZFT ages (22–18 Ma for Tambo/Suretta nappe). (3) The Adula nappe of the distal European margin shows a distinctly younger cooling history (dotted lines in Fig. 4). The steep exhumation path for the Adula nappe shows a major kink at 28–21 Ma indicating pronounced late Oligocene/early Miocene movement in the Alpine subduction channel.

### 3.3. Structure

The tectonic model of Schmid et al. (1996) explains the forward P-T breaks well, especially in the Helvetic domain. The Adula nappe shows evidence of top-N/NW directed thrusting postdating high-P metamorphism and facilitated the emplacement of the Adula nappe over the Simano and Leventina nappes (Rütti, 2003).

Backfolding and top-SE backshearing/backthrusting overprinting the early top-NW/N thrusts are an integral part of the Schmid et al. model. Backfolding/backthrusting is best illustrated by the Schams nappe, which roots in the northern Misox zone and is wrapped around the fronts of the Tambo and Suretta nappes (Schmid et al., 1990; Schreurs, 1993). Backfolding/backthrusting is considered as one and the same tectonic event related to post-collisional shortening and the formation of the southern steep belt in the Central Alps. The age of the backfolding/backthrusting event is not well known, but thought to have commenced by 35 Ma and continued into the Miocene (Schmid et al., 1990, 1996). Nievergelt et al. (1996) speculated that backfolding/backthrusting might be as old as 45 Ma. Hermann and Müntener (1992) observed that folding may have affected structures related to the Turba mylonite zone prior to the intrusion of the Bergell tonalite at ~32 Ma. The post-kinematic intrusion of acidic dykes associated with the Novate granite crosscut the Insubric mylonites in the southern steep belt at ~25–23 Ma (Liati et al., 2000) and document the end of ductile backthrusting and dextral shearing at the Insubric line.

Important for our study are the inverse P-breaks. The Austroalpine-Pennine boundary zone is considered the main target for major normal movements (Platt, 1986; Weh, 1998; Price et al., 2018). However, the P-T data demonstrate that the major metamorphic breaks occur below the Austroalpine-Pennine boundary zone sensu stricto, with P-break-1 cutting up section from the North Pennine Misox zone into the South Pennine domain between the Platta nappe and the Avers Bündnerschiefer (Figs. 2, 3). As mentioned above, P-break-1 is apparently folded by the N-closing Niemet-Beverin fold (Figs. 2, 3). The complementary S-closing fold above and east of the axial-trace of the Niemet-Beverin fold is obscured and truncated by the Turba mylonite zone (Nievergelt et al., 1996). Nievergelt et al. (1996) suggested that movement in the *E*-dipping, top-SE/E displacing Turba mylonite zone was coeval with late stages of the Niemet-Beverin folding phase. The Turba mylonite zone is parallel to P-break-1 for about 10–15 km and then cuts up section towards the N (Nievergelt et al., 1996) and is supposed to join up with the Gürgaletsch shear zone. Both shear zones are considered the most prominent low-angle normal faults in the Central Alps. A temperature gap of ~70°C between the hotter footwall and the cooler hanging wall has been estimated across the Turba mylonite zone (Nievergelt et al., 1996), suggesting a modest structural excision of ~2–3 km (Ring, 1992b). Nievergelt et al. (1996) envisaged an age of 45–30 Ma for the Turba mylonite zone. The lower age limit seems robust as the Turba mylonite zone affects the tonalite of the Bergell pluton and is truncated by the Bergell granodiorite (Liniger, 1992).

The Martegnas shear zone (Weh and Froitzheim, 2001) lies only a few kilometers below and west of the Turba and Gürgaletsch shear zones but above P-break-1 (Figs. 2, 3) and has also been interpreted as a low-angle normal fault. The top-SE displacing Martegnas shear zone mainly runs along the contact between the low-P Schams nappe and North Pennine flysch and then cuts down section to the S. Given the low-grade metamorphic conditions in both units, the displacement at the Martegnas shear zone appears modest or its dip angle was very low. However, the Martegnas shear zone brought the North Pennine flysch into its southerly position relative to the rest of the North Pennine sediments. Price et al. (2018) constrained the age of the Martegnas shear zone to >24 Ma. In the S, the Martegnas shear zone merges with the Turba mylonite zone (see Fig. 4 in Weh and Froitzheim, 2001). It appears that the Martegnas and Gürgaletsch shear zones are associated with the northern segment of P-break-2, which is cutting up-section to the N (Fig. 2).

Above the Turba mylonite zone, Liniger (1992) proposed another low-angle normal fault, the greenschist-facies top-E Corvatsch mylonite zone. The descriptions of Liniger (1992) combined with those of Mohn et al. (2011) suggest that major normal movement occurred before the Tertiary and is thus unrelated to the P-breaks discussed here. However, Price et al. (2018) showed a discontinuity in ZHe ages across the Corvatsch mylonite zone, indicating brittle reactivation of at least some segments of the fault in the Tertiary. Price et al. (2018) named these reactivated segments the Corvatsch detachment fault (Figs. 2, 3) and proposed that it splays off the Turba mylonite zone.

Below the Turba mylonite zone, distributed top-E mylonitic shearing has been described from the Tambo, Suretta and the eastern Adula nappes, as well as the Splügen and Misox zones separating those nappes (Löw, 1987; Ring, 1992b; Baudin et al., 1993; Pleuger et al., 2003). Baudin and Marquer (1993) argued that the top-E structures accommodated synkinematic decompression from 10 to 5 kbar in the Tambo nappe, suggesting that top-E shearing started at about 37 km depth and exhumed the rocks by ~18.5 km. One $^{40}Ar/^{39}Ar$ white-mica age of 35.7 ± 0.6 Ma from the Suretta nappe by Challandes et al. (2003) has been interpreted to date the waning stages of the decompression structures at greenschist-facies conditions. The top-E structures are prominent in the Misox zone where the P breaks merge.

The Forcola and Muretto faults, as well as the Engadine line are late faults that show mutual crosscutting relations with each other. The Engadine line cuts the Turba mylonite zone and the Muretto fault, and is itself cut by the Forcola fault (Fig. 2). Schmid and Froitzheim (1993) showed that relative movement along the Engadine line is complicated and involves E-W extension NE of St. Moritz and sinistral strike-slip faulting between St. Moritz and the Bergell intrusion, making it likely that the Engadine line is a composite structure. Further west, the Engadine line is obscured by diffuse ductile deformation, which accommodated rapid footwall uplift of its southern block immediately following the Bergell intrusion. Therefore, the western Engadine line is a top-N normal fault.

The Forcola fault (Weber, 1966) is a NE-dipping fault recording ENE-directed normal faulting (Ring, 1994b; Ciancaleoni and Marquer, 2008). It offsets the Tambo nappe in the hanging wall relative to the Adula nappe in the footwall by a throw of ~3 km (Meyre et al., 1998). The Forcola fault deforms the 24 ± 1.2 Ma Novate granite (Fig. 2). The post-Bergell Muretto fault is a dextral oblique-normal fault which is kinematically compatible with some minor faults immediately north and east of the Bergell pluton.

The Forcola and Muretto faults, as well as the Engadine line are largely coeval with the formation of the Cressim antiform, which is due to N-S shortening and folds the deep Helvetic nappes and the Bergell intrusion (Heitzmann, 1975) (Fig. 3). Overall, the structural relationships and the relationships with exhumation of the Bergell intrusion suggests that movement on these faults occurred during the late Oligocene to early Miocene.

## 4. Open questions and rationale for this study

A major open question is how the three inverse P-breaks above the Adula nappe relate to sustained top-N/NW thrusting and post-collisional backfolding/backthrusting? The only way those P-breaks could be produced by thrusting is via major out-of-sequence faulting (Wheeler and Butler, 1994; Bender et al., 2018). Peak P-T conditions in the Adula nappe are distinctly higher than those in the nappes above and below it. We therefore use the Adula nappe as a 'tectonic marker'. The Adula nappe was thrust onto the Simano and Leventina nappes and at this stage its overburden needs to have been reduced drastically to explain the forward P break of >10 kbar (cf., Ring and Kassem, 2007). The beginning of this thrusting is constrained by the age for initial exhumation of the Adula nappe at 34.2 ± 0.2 Ma (Hermann et al., 2006). In principle, the reduction of the overburden above the Adula nappe could be achieved by normal faulting, vertical ductile thinning or erosion (cf. Ring et al., 1999). Erosion as a major agent of exhumation can be ruled out as topography in the Alps was just building up at that time and cannot account for the removal of 10's of kilometers of crust within a short period of time explaining exhumation rates >15 km/Ma (cf., Platt, 1986). Kassem and Ring (2004) and Ring and Kassem (2007) showed that vertical ductile thinning associated with nappe stacking accounted for about 11–18 km (3–5 kbar) of overburden reduction in the Gran Paradiso massif of the Western Alps. Such figures are still not enough to explain the Adula/Simano nappe problem, especially since the nappe contact may have been dipping at 45° (Price et al., 2018) in which case an initially steep foliation should have formed. Hence, we conclude that there must have been normal shear zones above the Adula nappe, which aided the reduction of its overburden at about 34 Ma. Therefore, normal shear zones are related to the P-breaks above the Adula nappe.

However, the Turba mylonite zone, which is commonly considered the major normal fault in the eastern Central Alps (Nievergelt et al., 1996; Beltrando et al., 2010; Scheiber et al., 2012) runs oblique to the major P-breaks, especially P-break-1, and apparently only accounts for an offset of 2–3 km (Ring, 1992b). According to Baudin and Marquer (1993), the distributed, ductile top-E structures above the Adula nappe accomplished minimum exhumation of almost 20 km. If one assumed a 30° dip to the E, this would translate into minimum E-W displacement of about 40 km. A question is how distributed, ductile top-E normal shearing is related to the Turba mylonite zone?

Another open question is how the backfolding/backthrusting event starting at 45 or 35 Ma relates to exhumation above the Adula nappe and sustained top-N/NW thrusting in the eastern Central Alps (cf., Schmid et al., 1990, 1996). The tectonic model for backfolding/backthrusting (cf., Schmid et al., 1990) has been inspired by analogue models of Merle and Guillier (1989), who simulated post-collisional shortening across the Insubric line by two horizontally moving pistons. The model shows that a vertical velocity profile develops in the viscous material that is expelled laterally (to the N/NW) below the rigid orogenic lid (i.e., Austroalpine unit). Because the shortening was exerted by horizontal pistons, the N-closing Niemet-Beverin backfold has been modelled to have subhorizontal lower and upper limbs. In present coordinates, the upper and lower limbs of the backfolded Schams nappe are also subhorizontal and subparallel to each other. However, because the backfold is envisaged to have formed at 45–35 Ma, the nappe pile at this time was in the subduction channel and dipping at about 45° to the S/SE (see restoration in Price et al., 2018). Therefore, the limbs of the N-closing Niemet-Beverin backfold must have also dipped to the S/SE and top-SE 'backthrusting' was actually normal to the surface and would have contributed to the exhumation of the underlying nappes. In other words, the 'backthrust' would be a normal fault. A related question is how the Schams nappe could have rooted in the Misox zone between various high-P nappes, is associated and sandwiched between P-break-1 and 2, and has itself no indication for any high-P overprint?

The normal shear zones above the Adula nappe have shear directions to the E and SE and thus indicate, at least in part, out-of-plane deformation. If the P-breaks have been accomplished by normal shear zones, then the normal shear zones must have considerable displacement, which in turn indicates that the role of out-of-plane deformation is not negligible and should thus not be ignored in large-scale tectonic models. Tangential movements also have an impact on the cylindrical two-dimensional approaches to understand orogenic deformation in the Alps.

## 5. Kinematic analysis

We describe structural field data from three study areas at and below the Turba mylonite zone which allow to put the samples used for age dating into a tectonic context. The structures also relate directly to the three inverse P-breaks defined above, and in conjunction with the age data will help to reevaluatethe role of normal shear zones and tangential motion in the Central Alps. Note that we did not systematically map earlier thrust-related structures and focus on structures related to normal shearing and faulting.

### 5.1. Avers Bündnerschiefer

Fig. 5a provides a structural map of the Avers Bündnerschiefer and adjacent units, including the Turba and Avers mylonite zones, the Martegnas shear zone and P-break-1. In general, the main foliation dips moderately to the ENE (Fig. 5b). Only where the Middle Pennine cover is folded together with the Suretta basement in the NW, northerly dips occur. The mylonitic stretching lineations show distinct spatial patterns, which we describe from bottom to top. In the easternmost Suretta basement and overlying cover strip, stretching lineations are predominantly E/ENE trending (Fig. 5c) and associated with top-E shear-sense indicators. The top-E kinematic indicators pervasively affect geochronology sample Su13–7 and adjacent rocks. Sample Su13–7 (46°30′46"N, 9°27′24″E) is a tightly foliated, quartz-rich, fine-grained ultramylonite (Fig. 6a). Microscopically, the foliation is defined by strongly oriented and thoroughly recrystallized white mica, chlorite and mm-wide bands of aggregates of fully recrystallized quartz. These minerals also form the top-E kinematic indicators. Titanite occurs both as early- to syn-deformational porphyroblasts and as elongated aggregates in the foliation. With the exception of sparse albite porphyroclasts in white mica+chlorite-dominated shear bands, there is no evidence of pre-deformational textural relics in the rock. White mica shows a unimodal grain-size distribution. This sample will date top-E deformation at the top of the Middle Pennine nappe stack.

Further E, just below P-break-1 at the contact between the Avers Bündnerschiefer and the Schams nappe, there are mylonitic, SE-trending stretching lineations (Fig. 5d). We name this highly deformed zone the Avers shear zone. The penetrative SE-trending lineations continue southwards into the Turba mylonite zone. The stretching lineations are subparallel to axes of isoclinal folds (Fig. 7a), which have been correlated with the Niemet-Beverin backfold (Schreurs, 1993). Associated shear-sense indicators mainly provide a top-SE sense of shear (we analyzed 89 structures in detail and 68 of them provide top-SE shear sense; Fig. 7b, c) but top-NW fabrics (21 observations) (Fig. 7d) also occur. Quartz and white mica are severely recrystallized in the shear fabrics. Mylonite samples Su13–8, Be14–12 and Be14–13 were collected from this broad (about 300–800 m wide) shear zone. All samples date top-SE mylonitic shearing. Sample Su13–8 from the Avers mylonite zone (46°28′40"N, 9°29′52″E), is a fine- to medium-grained, carbonate+quartz-dominated mylonite. Microscopically, deformation is inhomogeneously distributed. It is focused into mm-wide, white-mica-rich shear bands in which the rock is distinctly finer grained than away from these shear bands, where white mica is also less abundant. Quartz occurs within the foliation as well as in strain shadows of large (up to 5 mm) sulphide crystals. These sulphide crystals, and also big quartz crystals rimmed by recrystallized grains, possibly constitute pre-deformational textural relics. Pre-deformational textural relics are not

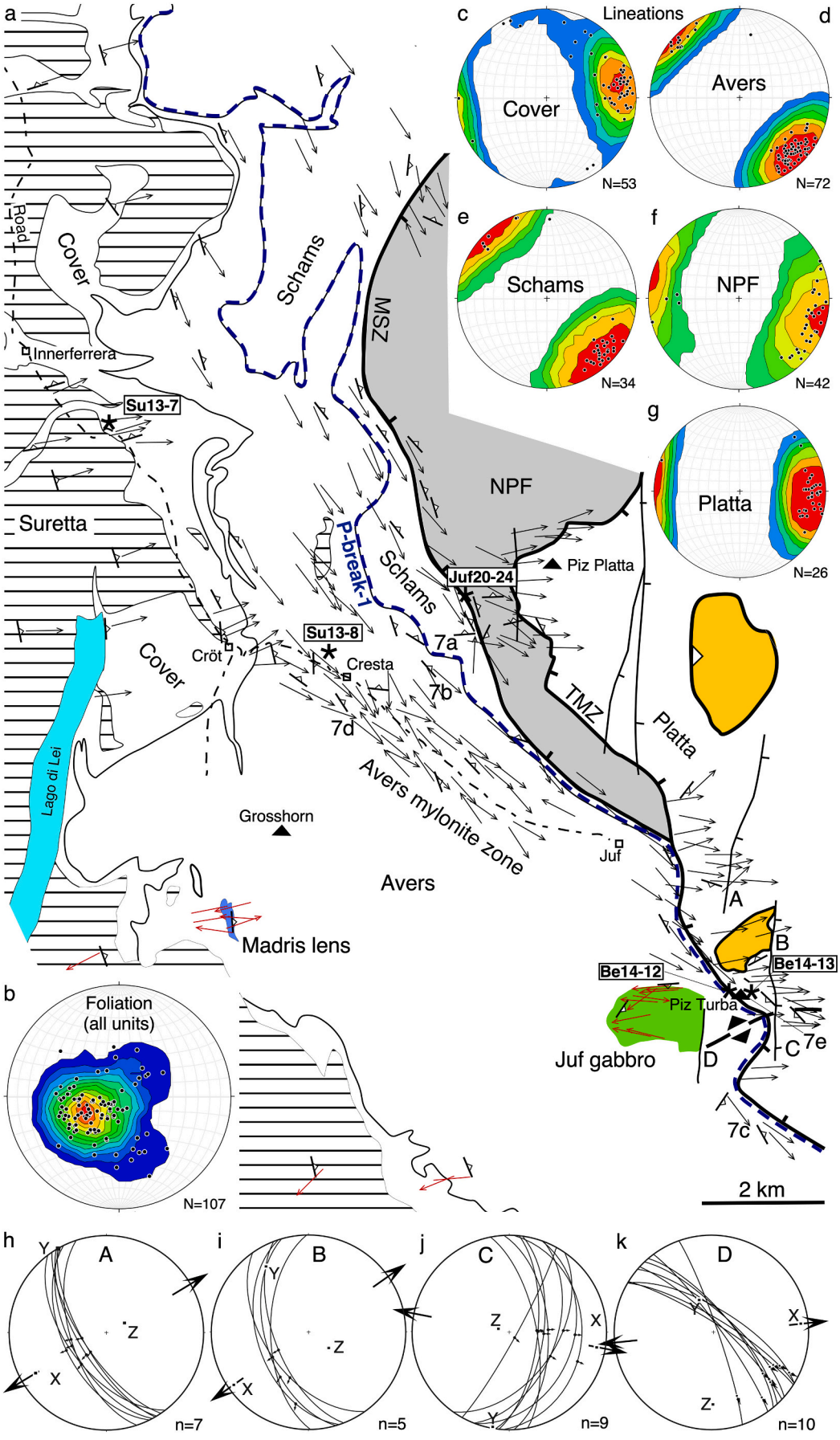


**Fig. 5.** (a) Tectonic map of the Avers Bündnerschiefer and adjacent nappes with Martegnas shear zone (MSZ), Turba mylonite zone (TMZ) and P-break-1 on top of high-P Avers Bündnerschiefer against lower greenschist-facies Schams and Platta nappes and North Pennine flysch (NPF) (map modified from Staub, 1926; Liniger, 1992; Schreurs, 1993; Scheiber et al., 2012); refer to Fig. 2 for location of map, pattern for Suretta nappe and colour scheme; the North Pennine flysch and the Margna-Sella nappe indicated for aiding orientation. The SE-trending stretching lineations in the upper parts of the Avers Bündnerschiefer define a broad top-SE shear zone. Note that earlier W-trending stretching lineations (in red) associated with top-W kinematic indicators occur in the Madris blueschist lens and the Juf gabbro. Also shown are sample locations for Su13–7, Su13–8, Be14–12, Be14–13 and Juf20–24 and localities of photos (a) to (e) in Fig. 7. The arrow heads of the stretching lineations indicate the direction of movement of tectonic top. (b) Foliation planes with data from all units shown on map showing shallow to moderately ENE-dipping planes. (c) Stretching lineations from the Suretta nappe and its cover showing strong ENE-plunging maximum. (d) Stretching lineation data from the Avers Bündnerschiefer depicting pronounced SE-plunging lineations. (e) Stretching lineations in the Schams nappe show same pattern as in the Avers Bündnerschiefer with a strong SE-plunging maximum. (f) Stretching lineations from the North Pennine flysch display some scatter between SE- and E-plunging lineations. (g) The stretching lineations in the Platta nappe show an E-plunging set. (h-k) Fault-slip analysis of N-striking normal faults around Piz Turba providing NE-SE (h, i) and E-W (j, k) extension directions. (For interpretation of the references to colour in this figure legend, the reader is referred to the web version of this article.)

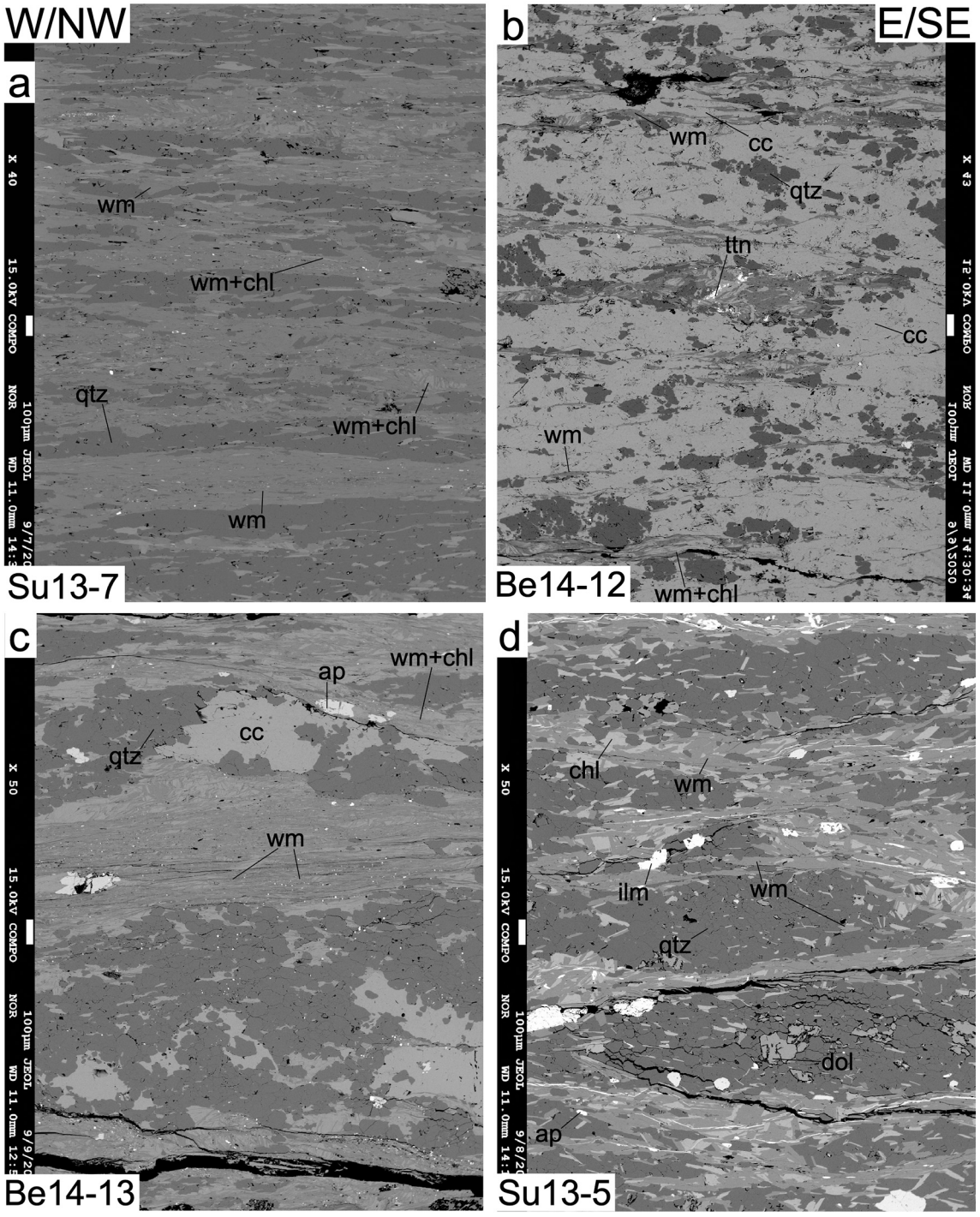


**Fig. 6.** Backscattered electron images of some samples used for Rb—Sr dating. (a) Su13–7 is a fine-grained ultramylonitic rock, which is texturally fully equilibrated during ductile shearing. Note the absence of any textural relics, porphyroclasts or discrete shear bands (Rb—Sr isochron in Fig. 10h). (b) Sample Be14–12 containing fine-grained white mica. Chlorite is intergrown with minor carbonate, both co-defining shear bands which alternate at the mm scale with more coarse-grained, carbonate+quartz-dominated layers (Rb—Sr isochron in Fig. 10b). (c) Sample Be14–13; all white mica and carbonate grains are fully recrystallized during top-SE shearing. There are no obvious pre-deformation relics of the age-defining subassemblage of carbonate + white mica (for Rb—Sr isochron see Fig. 10a). (d) Sample Su13–5 characterized by large white-mica crystals within texturally late shear bands. Smaller grains of white mica occur within less strongly sheared, texturally earlier lensoidal domains (see Fig. 10f for Rb—Sr isochron). Small vertical, white scale bars represent 100 μm; abbreviations: ap = apatite, cc = calcite, chl = chlorite, dol = dolomite, ilm = ilmenite, wm = white mica, qtz = quartz, ttn = titanite.

evident in the white-mica population. Samples Be14–12 and Be14–13 from the Turba mylonite zone (46°24′24″N, 9°37′25″E) are fine-grained, equigranular carbonate mylonites (Fig. 6b, c). The deformation fabric is defined by white mica, chlorite, and strongly elongated quartz-carbonate aggregates. Microscopically, deformation-induced recrystallization is pervasive delineating a particularly tight foliation. Pre-deformational textural relics are not observed. White mica is rare but distinctly enriched in shear bands. Occasionally the foliation is cut at high angles by quartz-carbonate-filled extension veins with fibers parallel to the SE-trending stretching lineation (Fig. 7e).

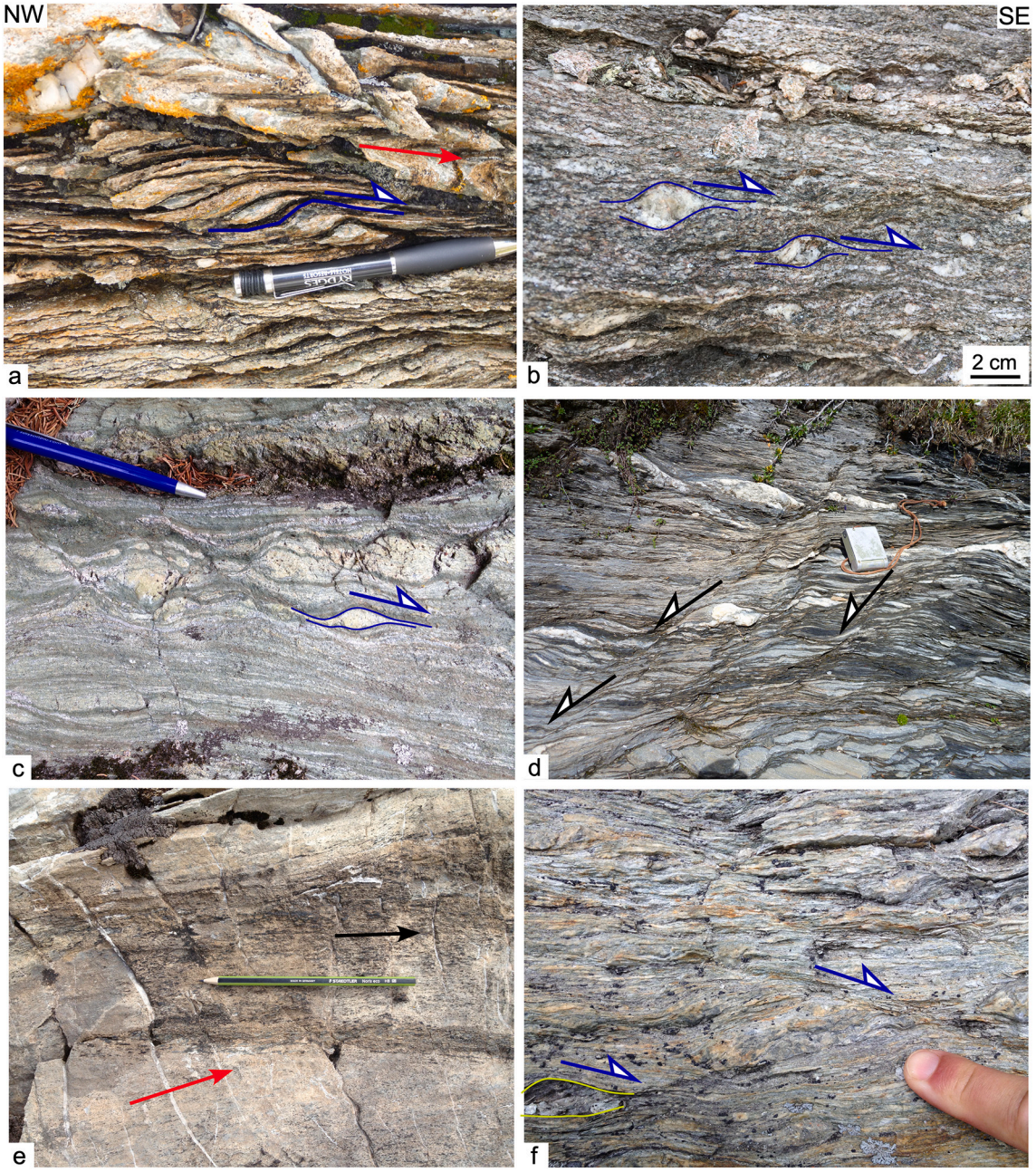


**Fig. 7.** (a) S-C-type shear-band fabric (highlighted in blue) in calcschist at the contact of the Avers Bündnerschiefer and the Schams nappe. The fold axes in the upper right (red arrow parallels down-plunge direction of fold axis) have axes subparallel to the stretching lineation. (b) Top-SE sigma casts in Avers Bündnerschiefer (marked by blue lines and arrow). (c) Asymmetric, boudinaged epidote-rich layers in greenschist of the Avers Bündnerschiefer indicating top-SE sense of shear (marked by blue lines and arrow). (d) Top-NW shear bands (marked by black arrows) in Avers Bündnerschiefer. (e) SE-trending stretching lineation on mylonitic foliation plane of sample Be14–13. Note that the stretching lineations (black arrow) trend 133° and the fibers in the extensional veins (red arrow) trend 111°. (f) Top-ENE shear bands in Vals Bündnerschiefer of the Misox zone (marked by blue lines and arrow) very near the locality for sample Be14–7. (For interpretation of the references to colour in this figure legend, the reader is referred to the web version of this article.)

In the Schams nappe, similarly oriented SE-trending stretching lineations were mapped (Fig. 5e). These stretching lineations become semi ductile and cataclastic in appearance in the Martegnas shear zone and the overlying North Pennine flysch. Sample Juf20–24 from the Martegnas shear zone (46°28′59″N, 9°32′25″E) is a fine-grained, equigranular, mylonitic greenschist collected directly at the contact between the Schams nappes and the North Pennine flysch. Microscopically, the deformation fabric is defined by recrystallized white mica, chlorite, and strongly elongated quartz aggregates and shows top-SE shear sense. In general, the lineations in the Martegnas shear zone are associated with top-SE kinematic indicators (46 observations) but we also mapped some top-NW shear-sense indicators (11 observations). Within the North Pennine flysch, the stretching lineations show some scatter, rotate into an easterly direction (Fig. 5f) and are associated with top-E shear-sense indicators. In the Platta nappe above the Turba mylonite zone, the stretching lineations have a well-defined easterly trend (Fig. 5g) and the kinematic indicators are top-E.

The Turba mylonite zone shows a distinct mismatch in the orientation of the stretching lineations, with SE-trending stretching lineations below and E-trending ones above it (Fig. 5a) (see also Nievergelt et al., 1996). South of Piz Turba, Liniger (1992) mapped a late antiform which folds the Turba mylonite zone. This antiform and the Turba mylonite

zone are then cut by steep, E-dipping normal faults (Liniger, 1992), which are not folded and therefore not related to the folded Turba mylonite zone (Ring, 1994b). Most normal faults provide a NE-trending extension direction (Fig. 5h, i), only station C from S of Piz Turba supplies an E-W-directed extension direction (Fig. 5j). The contact of the Turba mylonite zone with the Juf gabbro has been overprinted by a steeply ENE-dipping dextral oblique slip normal fault also providing an E-W extension direction (Fig. 5k).

In the Madris blueschist lens and the Juf gabbro (Fig. 5a), early W-trending stretching lineations (Fig. 5a) associated with top-W shear-sense indicators occur in thin layers that escaped a widespread greenschist-facies overprint. In the Madris blueschist, glaucophane, phengite, epidote, chlorite and quartz are stable in the shear fabrics. The blueschist layers occur within greenschist and in the latter the stretching lineations are scattered, trend E-W to NW-SE and are associated with top-NW shear-sense indicators. In large parts, the Juf gabbro is mylonitically deformed in subhorizontal shear zones associated with top-W kinematic indicators. In places, the gabbro is undeformed and coarse grained with up to 5-mm-large augite crystals occurring in a whitish-greenish matrix largely made up by saussuritized plagioclase. In mylonitic gabbro, augite is occasionally rimmed by actinolite; plagioclase is commonly replaced by albite, clinozoisite, pumpellyite and sericite.

### 5.2. Splügen zone

The Splügen zone between the Tambo and Suretta basement nappes is made up by basal conglomerate, quartzite and dolomite, which are overlain by strongly sheared and imbricated Triassic marble (Figs. 2, 8a) (Blanc, 1965; Ring, 1992a; Baudin et al., 1993; Scheiber et al., 2012). The mylonitic marble dips shallow to moderately to the E (Fig. 8b) and contains white mica defining a penetrative stretching lineation associated with top-E kinematic indicators (Ring, 1992b; Baudin et al., 1993; Marquer et al., 1996). Our sample from the Splügen zone, Su13–5 (46°28′17″N, 9°21′08″E), is a tightly foliated, quartz-rich mylonite associated with top-E shear sense indicators. Microcopically, the foliation is defined by recrystallized, oriented chlorite+quartz bands (Fig. 6d). Particularly large grains of white mica are seen in texturally late shear bands. Fine-grained, lens-shaped aggregates of quartz and fine-grained white mica are separated from each other by shear bands rich in white mica. Albite is not abundant, fully recrystallized, and forms part of quartz-rich domains.

The rocks of the overlying Suretta nappe also dip to the E (Fig. 8b) and show the same E-trending stretching lineation (Fig. 8c), which in part overprints a NNW-trending lineation (Ring, 1992b; Baudin et al., 1993; Marquer et al., 1996; Scheiber et al., 2012). Phengite making up the E-trending stretching lineation shows a systematic decrease in Si content, which Baudin and Marquer (1993) interpreted to indicate that the stretching lineation formed during exhumation from 10 to 5 kbar. Associated with the E-trending stretching lineation are top-E kinematic indicators. Sample Su13–3 (46°30′27″N, 9°20′22″E) is a mylonite with large (up to 2 mm) porphyroclasts of feldspar (mainly K-feldspar) in a fine-grained, tightly foliated matrix consisting of quartz, feldspar, minor epidote, white mica and chlorite. Whereas the feldspar population comprises pre-deformational relics, as evident from a bimodal grain-size distribution, the grain-size distribution of white mica is unimodal. All white mica belongs to the fine-grained recrystallized subassemblage associated with top-E kinematic indicators.

### 5.3. Misox zone

The rocks of the Misox zone belong to the Vals Bündnerschiefer and separate the Adula nappe of the distal European margin from the Middle Pennine Tambo basement nappe (Figs. 2, 9a). It contains calcschist (Bündnerschiefer), greenschist, metagabbro and impure marble (Gansser, 1937; Probst, 1980). The upper boundary to the Adula nappe is the Pescion zone (Gansser, 1937; Pleuger et al., 2003), a diverse zone

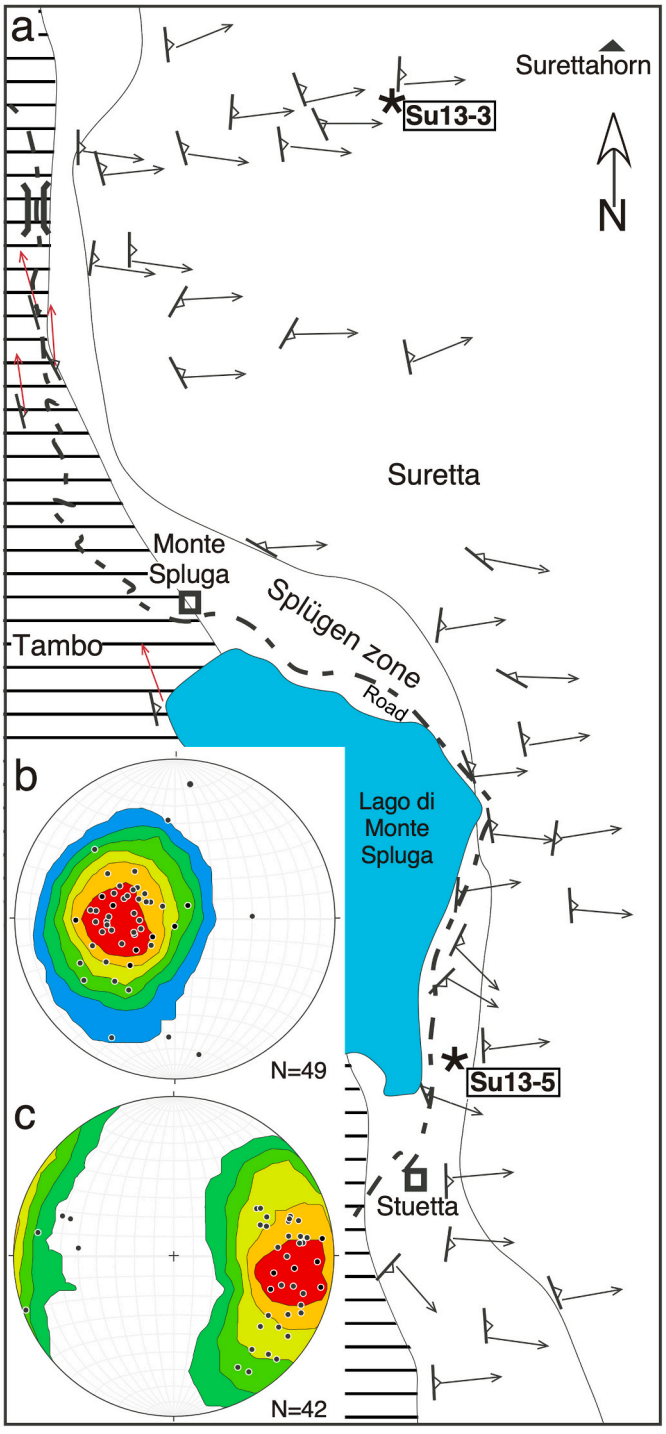


**Fig. 8.** (a) Simplified structural map of the Splügen zone. Note that the Knorren mélange, consisting of paragneiss, impure marble, quartzite and a gneissic breccia, has been lumped together with the northeastern Tambo nappe. Refer to Fig. 2 for the location of the map and the pattern for Tambo nappe. Early NNW-trending stretching lineations (in red) have hardly been mapped and are not shown in the stereonet. The second set of stretching lineations trends about E-W. (b) The foliation planes show gentle to moderate easterly dips. (c) The stretching lineations are E- to SE-plunging with an easterly maximum. (For interpretation of the references to colour in this figure legend, the reader is referred to the web version of this article.)

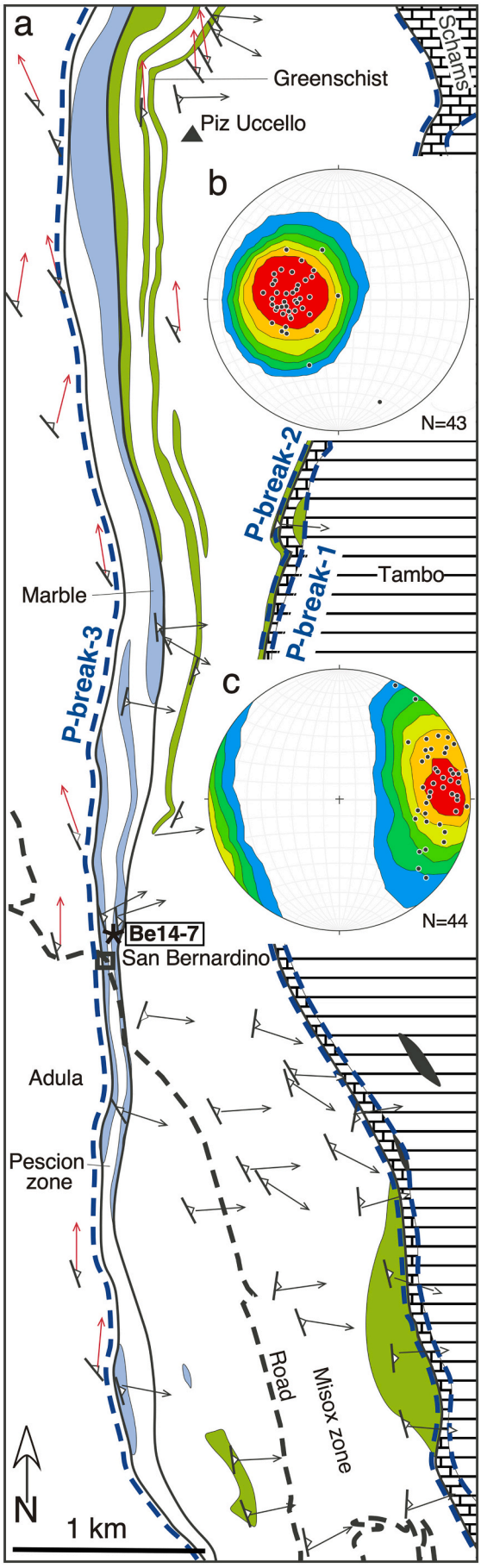


(caption on next page)

**Fig. 9.** (a) Simplified structural map of the Misox zone (from Gansser (1937), Pleuger et al. (2003), and own mapping). Refer to Fig. 2 for the location of map; the patterns for the Tambo and Schams nappe are indicated for aiding orientation on the map and are as in Fig. 2. Early NNW-trending stretching lineations (red) more dominant in Adula nappe and Pescion zone to the W, the E-plunging stretching lineations are abundant in the eastern Misox zone and the Tambo nappe. (b) The foliation planes show a similar pattern as in the Splügen zone and Avers region with gentle to moderate dips to the E. (c) The stretching lineations show a distinct E-plunging maximum (note that earlier NNW-trending stretching lineations are not shown for clarity). (For interpretation of the references to colour in this figure legend, the reader is referred to the web version of this article.)

of gneiss from the Adula nappe, dolomitic marble, calcschist, cargneule (yellow-brown, de-dolomitized breccia) and greenschist. Above the Misox zone, a narrow strip of Schams nappe has been mapped below the Tambo nappe (Pleuger et al., 2003). As mentioned above, all three inverse P-breaks converge and root in the Misox zone (Fig. 9a).

The oldest set of stretching lineations is NNW-trending. In the northern part of the Adula nappe, E-trending stretching lineations associated with an E-dipping foliation strongly overprint earlier structures (Fig. 9b, c) (Löw, 1987; Ring, 1992b). Sample Be14–7 (46°46′28"N, 9°11′29″E) is a fine-grained carbonate mylonite with strong, near-pervasive recrystallization associated with top-ENE kinematic indicators. Microscopically, the foliation is defined by oriented white mica together with elongated aggregates of calcite. There is a unimodal grain-size distribution for both calcite and white mica. In contrast, the feldspar population is dominated by a fine-grained generation, but pre- to early-deformational porphyroclastic, coarse-grained (mm sized) aggregates of feldspar are present as well. The top-E kinematic indicators are most pervasively developed in greenschist-facies rocks. The mylonitic character of the foliation and the stretching lineation increases upward towards the Tambo nappe. Shear-sense indicators indicate top-E shearing (see also Ring, 1992b; Baudin and Marquer, 1993; Pleuger et al., 2003) (Fig. 7f).

### 5.4. Summary

The top-SE displacing Avers shear zone occurs at the top of the Avers Bündnerschiefer and is parallel the Turba mylonite zone (Fig. 5a). It postdates a set of blueschist-facies stretching lineations. The relative age of the top-SE Martegnas shear zone is debatable but >24 Ma (Price et al., 2018). It has the same shear direction as the Avers mylonite zone, which may suggest that both shear zones are of the same age.

Mylonitic top-E shearing heterogeneously affected a broad zone above the Adula nappe which involves all units between the Misox zone at the bottom and the cover sediments of the Suretta nappe at the top. Baudin et al. (1993) proposed that this event was associated with a reduction in pressure from 10 to 5 kbar in the Tambo nappe. Brittle top-E normal faulting affected the rocks of the North Pennine flysch above the Martegnas shear zone, the Platta nappe above the Turba mylonite zone, and the Corvatsch detachment fault (Price et al., 2018). Some late normal faults record top-NE/SE normal faulting.

Below we report eight new Rb—Sr ages of mylonites for shedding more light on the ages of the discussed shear zones. Samples Be14–12, Be14–13 and Su13–8 will date top-SE shear in the Avers and Turba mylonite zones, and sample Juf20–24 top-SE shear in the Martegnas shear zone. Samples Be14–7, Su13–5, Su13–3 and Su13–7 belong, from bottom to top, to the zone of distributed top-E shear above the Adula nappe.

## 6. Rb—Sr geochronology

### 6.1. Rationale and analytical protocols

Rb—Sr multimineral dating is a powerful method to constrain the late stages of ductile deformation in mylonitic rocks. The Rb—Sr isotopic clock is set at the end of simultaneous recrystallization processes of high-Rb/Sr minerals (mica phases, K-feldspar) in equilibrium with coexisting low-Rb/Sr phases like plagioclase or apatite. Isochron ages directly date deformation, provided that no later retrogressive or thermal-diffusive overprint occurred (Inger and Cliff, 1994; Freeman et al., 1998). Muscovitic-phengitic white mica is particularly useful because resetting of its Rb—Sr system via diffusion at static conditions is possible only at temperatures well above 600°C (Glodny et al., 2008b), whereas dynamic recrystallization effectively resets the Rb—Sr system in white mica in many lithologies at temperatures as low as ~300°C (Müller et al., 1999). Mica is typically analyzed in several grain-size fractions to test for the potential presence of pre-mylonitic mica porphyroclasts that escaped from complete recrystallization. Since the ductile shear strength of minerals is grain-size sensitive (Platt and Behr, 2011), large mica crystals tend to form textural and isotopic relics whereas strain is preferentially partitioned into trails of fine-grained material. This results in more efficient isotopic re-equilibration of smaller grains, particularly during late stages of ductile deformation. Apparent ages of small-grain-size mica fractions thus correspond most closely to the latest stages of ductile overprint in a given sample. Absence of systematic correlations between mica grain sizes and apparent ages indicate penetrative recrystallization, resulting in a complete reset of the Rb—Sr mineral ages, and facilitating straightforward dating of the mylonitization event.

For mineral separation, we used small samples of less than 100 g, to avoid larger-scale compositional and isotopic heterogeneities. Rb—Sr isotopic data were generated at GFZ Potsdam on a ThermoScientific TRITON TIMS instrument. Sr isotopic compositions were measured in dynamic multicollection mode, whereas Rb isotope dilution analyses were done in static multicollection mode. The value obtained for $^{87}Sr/^{86}Sr$ in the NIST SRM 987 reference material during the period of analytical work was 0.710242 ± 0.000020 (2σ, $n = 16$). For calculation of isochron parameters, standard uncertainties of ±0.005% for Sr isotopic ratios and of ±1.5% for Rb/Sr ratios were used, provided that analytical uncertainties were smaller than these values. Else, analytical uncertainties were directly used as input parameters for age calculation. Handling of mineral separates and analytical procedures are described in more detail in Glodny et al. (2008a). Uncertainties of isotope and age data are quoted at 2σ throughout this work. The program ISOPLOT/EX3.71 (Ludwig, 2009) was used to calculate regression lines. The $^{87}Rb$ decay constant is used as recommended by Villa et al. (2015).

### 6.2. Electron-probe microanalysis

To better characterize the white-mica populations and mineral intergrowth relationships of the dated samples (Montemagni et al., 2020 and references therein), electron-probe microanalyses (EPMA) were performed with a JEOL-JXA 8530F probe at GFZ Potsdam, under common analytical conditions of 15 kV acceleration voltage, typically 10 nA beam current, wavelength-dispersive spectroscopy mode, using a 5 to 10-μm-diameter beam. The following standards were used for calibration: albite (Si, Al, Na), orthoclase (K), fluorite (F), rutile (Ti), diopside (Ca, Mg), tugtupite (Cl), and hematite (Fe). The quantitative analyses focused on phengite, because the phengite Rb—Sr system is crucial for age determination, whereas the Si atoms content per formula unit (apfu; calculated for 22 oxygen atoms) of phengite and the corresponding content of the celadonite endmember, $K(Mg,Fe^{2+})AlSi_4O_{10}(OH)_2$, can be used to distinguish between different mica subpopulations. The celadonite content of phengite may also be an indicator of relative pressure changes (Massonne and Schreyer, 1987), with higher Si contents pointing to higher P conditions of phengite (re)crystallization. Phengite and phlogopite microprobe analyses are presented in Table S1 in the Supplementary Material.

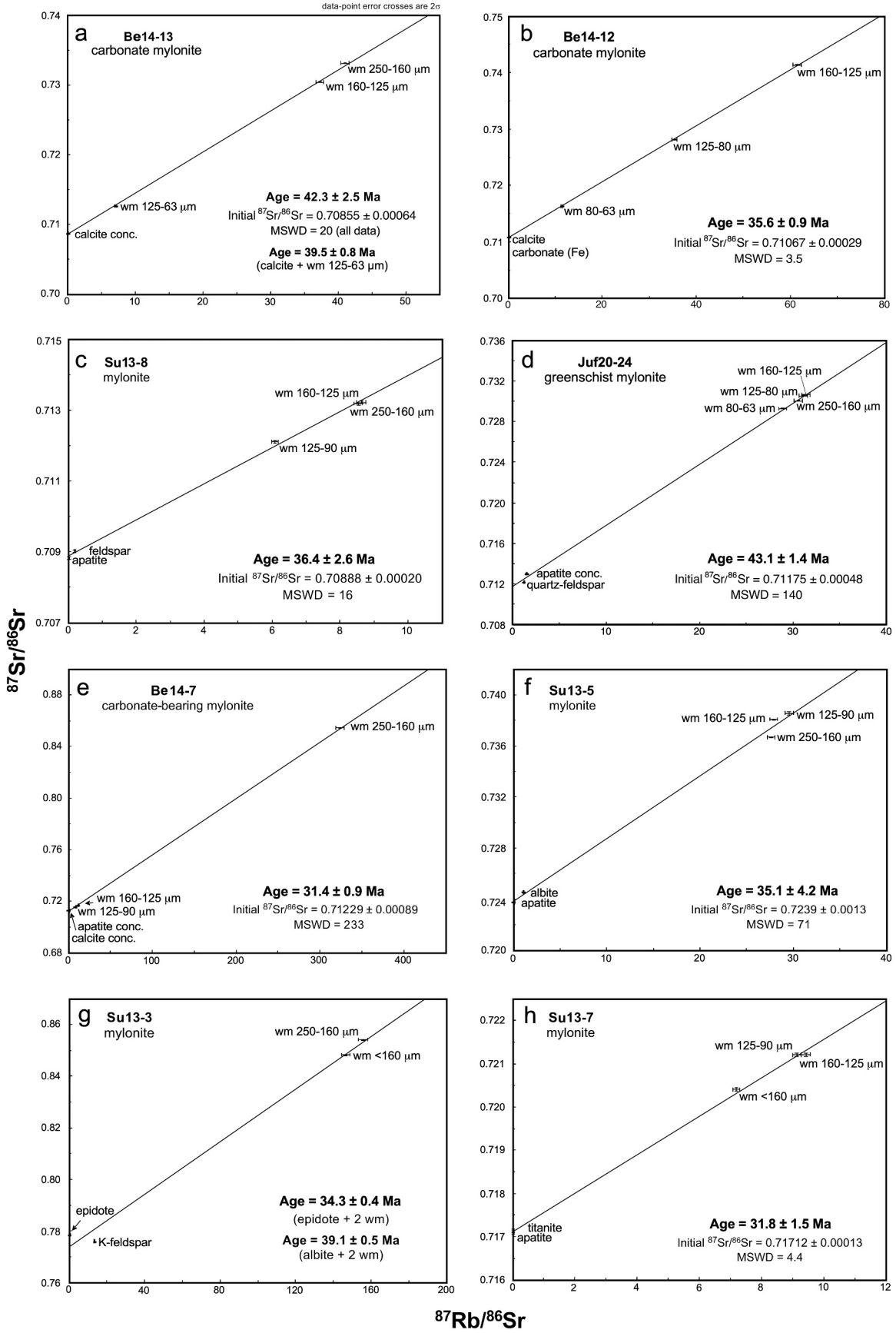


**Fig. 10.** Rb—Sr ages; wm = white mica, conc. = concentrate, MSWD = mean square weighted deviations.

**Table 2**
Rb—Sr isotopic data.

| Sample no. | Material | Rb (ppm) | Sr (ppm) | $^{87}Rb/^{86}Sr$ | $^{87}Sr/^{86}Sr$ | $^{87}Sr/^{86}Sr$ $2s_m$ (%) |
|---|---|---|---|---|---|---|
| **BE14–13** (42.3 ± 2.5 Ma; MSWD = 20) | | | | | | |
| PS2627 | wm 250–160 μm | 312 | 22.1 | 41.1 | 0.733104 | 0.0026 |
| PS2628 | calcite conc. | 10.9 | 337 | 0.0938 | 0.708727 | 0.0012 |
| PS2629 | wm 160–125 μm | 312 | 24.2 | 37.3 | 0.730362 | 0.0014 |
| PS2630 | wm 125–63 μm | 223 | 90.3 | 7.16 | 0.712625 | 0.0021 |
| **SU13–8** (36.4 ± 2.6 Ma; MSWD = 16) | | | | | | |
| PS2339 | apatite | 6.89 | 922 | 0.0216 | 0.708821 | 0.0009 |
| PS2340 | feldspar | 9.83 | 151 | 0.188 | 0.709025 | 0.0047 |
| PS2341 | wm 250–160 μm | 430 | 144 | 8.62 | 0.713216 | 0.0027 |
| PS2342 | wm 160–125 μm | 427 | 145 | 8.54 | 0.713180 | 0.0013 |
| PS2343 | wm 125–90 μm | 417 | 199 | 6.08 | 0.712108 | 0.0046 |
| **SU13–3** (34.3 ± 0.4 Ma; MSWD = 3.2) | | | | | | |
| PS2344 | epidote conc. | 63.9 | 1640 | 0.113 | 0.778465 | 0.0007 |
| PS2345 | wm 250–160 μm | 862 | 16.2 | 156 | 0.854099 | 0.0055 |
| PS2346 | wm <160 μm | 881 | 17.6 | 147 | 0.848321 | 0.0050 |
| PS2348 | K-feldspar | 161 | 34.7 | 13.5 | 0.775928 | 0.0042 |
| **SU13–5** (35.1 ± 4.2 Ma; MSWD = 71) | | | | | | |
| PS2349 | apatite | 4.68 | 913 | 0.0149 | 0.723742 | 0.0009 |
| PS2350 | wm 125–90 μm | 356 | 35.0 | 29.5 | 0.738570 | 0.0180 |
| PS2351 | wm 160–125 μm | 368 | 38.3 | 27.9 | 0.738070 | 0.0020 |
| PS2352 | albite | 9.53 | 25.9 | 1.07 | 0.724556 | 0.0022 |
| PS2353 | wm 250–160 μm | 348 | 36.5 | 27.6 | 0.736671 | 0.0023 |
| **SU13–7** (31.8 ± 1.5 Ma; MSWD = 4.4) | | | | | | |
| PS2468 | apatite | 1.43 | 566 | 0.00731 | 0.717102 | 0.0011 |
| PS2469 | titanite | 2.05 | 344 | 0.0172 | 0.717143 | 0.0014 |
| PS2470 | wm >160 μm | 384 | 155 | 7.19 | 0.720403 | 0.0012 |
| PS2471 | wm 125–90 μm | 420 | 130 | 9.37 | 0.721218 | 0.0035 |
| PS2472 | wm 160–125 μm | 413 | 131 | 9.13 | 0.721200 | 0.0024 |
| **BE14–7b** (31.4 ± 0.9 Ma; MSWD = 233) | | | | | | |
| PS2660 | apatite conc. | 8.79 | 166 | 0.154 | 0.712631 | 0.0017 |
| PS2661 | calcite conc. | 7.95 | 49.6 | 0.464 | 0.713094 | 0.0033 |
| PS2662 | wm 160–125 μm | 235 | 59.0 | 11.5 | 0.716734 | 0.0024 |
| PS2663 | wm 125–90 μm | 194 | 68.3 | 8.22 | 0.715570 | 0.0030 |
| PS2664 | wm 250–160 μm nm | 263 | 2.38 | 324 | 0.854426 | 0.0024 |
| **JUF 20–24** (43.1 ± 1.4 Ma; MSWD = 140) | | | | | | |
| PS3579 | wm 125–80 μm | 186 | 17.2 | 31.4 | 0.730628 | 0.0012 |
| PS3580 | wm 80–63 μm | 151 | 15.2 | 28.9 | 0.729263 | 0.0015 |
| PS3581 | quartz-feldspar | 5.37 | 12.7 | 1.23 | 0.712173 | 0.0011 |
| PS3582 | wm 160–125 μm | 194 | 18.0 | 31.1 | 0.730532 | 0.0017 |
| PS3583 | wm 250–160 μm | 189 | 17.9 | 30.6 | 0.730034 | 0.0020 |
| PS3584 | apatite conc. | 25.2 | 47.2 | 1.54 | 0.712997 | 0.0020 |
| **BE14–12** (35.6 ± 0.9 Ma; MSWD = 3.5) | | | | | | |
| PS3585 | carbonate (Fe) | 18.2 | 537 | 0.0979 | 0.710774 | 0.0016 |
| PS3586 | calcite | 6.50 | 77.7 | 0.242 | 0.710856 | 0.0016 |
| PS3587 | wm 160–125 μm | 343 | 16.2 | 61.5 | 0.741532 | 0.0021 |
| PS3588 | wm 125–80 μm | 343 | 28.1 | 35.5 | 0.728091 | 0.0016 |
| PS3589 | wm 80–63 μm | 296 | 74.3 | 11.5 | 0.716301 | 0.0015 |

Abbreviations: wm, white mica; conc, concentrate (slightly impure mineral separate); nm, nonmagnetic on Frantz magnetic separator at 1.2A/13°, indicating presence of particularly Fe-poor muscovite.

### 6.3. Results

For samples Be14–13 and Be14–12 (top-SE Turba mylonite zone) we obtained ages of 42.3 ± 2.5 Ma and 35.6 ± 0.9 Ma (Fig. 10a, b, Table 2). For sample Be14–13, the regression line is defined by Rb—Sr data for calcite and three grain-size fractions of white mica (Fig. 10a). There is a significant positive correlation between white-mica grain size and apparent age, with data for the biggest grain-size mica fraction plotting slightly above and data for the smallest grain-size fraction slightly below the regression line (Fig. 10a). We therefore argue that the age of 39.5 ± 0.8 Ma, calculated using calcite and white mica 125–63 μm, is the best age estimate for the end of ductile deformation in this sample. Microtextural observation indicates that albite forms clasts, interpreted as textural relics from an earlier metamorphic stage of the rock. However, the age-defining subassemblage, i.e., all white mica and carbonate grains, are fully recrystallized during top-SE shearing and no obvious pre-deformation relics occur in the shear fabrics (Fig. 6c). This is in line with the fairly narrow range of Si in phengite between 6.48 and 6.66 apfu (Table S1), which is also not correlated with the textural position of phengitic white mica. Hence, the age of 42.3 ± 2.5 Ma most probably dates earlier increments of top-SE shearing. It therefore appears likely that top-SE shearing commenced before 44.8 Ma and that 38.7 Ma represents a maximum age for the end of this shearing. This result is consistent with the age data obtained from sample Be14–12, which is from a slightly different position within the Turba mylonite zone. Data for calcite, Fe-bearing carbonate and three grain-size fractions of white mica define an age of 35.6 ± 0.9 Ma (Fig. 10b). Microtextural observations reveal that white mica and chlorite co-define shear bands, alternating at the mm scale with carbonate/quartz-dominated layers (Fig. 6b). There is a pronounced positive correlation between white-mica grain size and Rb/Sr ratio (Fig. 10b), pointing to presence of chemically distinct white-mica subpopulations within the sample. This is also suggested by the rather wide range of Si contents in phengite (between 6.50 and 6.79, Table S1). However, the Rb—Sr data for white

mica are well aligned on the regression line (Fig. 10b), indicating that the different mica characteristics were formed within a short period of time, in the range of the uncertainty of the Rb—Sr age. It appears that there is slight Sr-isotopic disequilibrium between the two carbonate fractions, as indicated by the MSWD (mean squared weighted deviation) of regression of 3.5. Potentially this minor but detectable disequilibrium is related to the texturally late formation of calcite-filled veinlets. Nevertheless, the age information is insensitive to the carbonate disequilibrium. Given the pronounced deformation fabric combined with microscopically observed penetrative synkinematic recrystallization of the age-defining carbonate/white mica subassemblage, the age of 35.6 ± 0.9 Ma is best interpreted to directly date the end of ductile deformation in that sample. In summary, results from the two samples Be14–12 and Be14–13 point to increments of ductile deformation within the Turba mylonite zone between 44.8 and 34.7 Ma.

Sample Su13–8 (top-SE Avers mylonite zone) provides an age of 36.4 ± 2.6 Ma (Fig. 10c). There is no perfect isochron correlation, but slight isotopic disequilibria both between different white-mica grain-size fractions, and between apatite and feldspar. The observed disequilibria are possibly related to in the microscopically observed presence of pre-deformational sulphide and quartz relics with their strain shadows, combined with the marked strain partitioning into distinct mica-rich shear bands. The majority of white mica in this sample is, with the exception of some crystal rims and small crystals in shear bands, compositionally a high-Si phengite, with Si apfu between 6.60 and 6.85. Larger white-mica crystals also show some compositional zoning, with Si up to 6.89 apfu in cores, and down to 6.40 apfu in rims (Table S1). This pattern potentially indicates prolonged, non-penetrative shearing during decreasing pressure conditions. In any case, the age information is, within limits of uncertainty, reliable and top-SE shear was underway in the Avers mylonite zone by 39 Ma.

Sample Juf20–14 (top-SE Martegnas shear zone) is a fine-grained mylonite dominated by very fine-grained white mica (estimated to >80% by volume) with a unimodal grain-size distribution. Pre-deformational relics of larger white-mica crystals are not observed. Rb—Sr data for an apatite concentrate, quartz-feldspar and four grain-size fractions of white mica yield an age of 43.1 ± 1.4 Ma (Fig. 10d). The elevated MSWD of 140 is due to apparent Sr-isotopic disequilibrium between the apatite and quartz-feldspar concentrates, whereas white mica shows a Sr-isotopically homogeneous population (Fig. 10d). The reason for disequilibrium remains unclear. Potentially apatite has been affected by processes induced by weathering-related oxidation of pyrite in the sample, as indicated by brownish staining on some apatite. The age information is, within limits of uncertainty, reliable and dates the end of top-SE ductile shearing.

Sample Be14–7 (Misox zone, top-E kinematics) shows textural evidence for non-pervasive recrystallization during late stages of mylonitization, like the scattered occurrence of porphyroclastic feldspar aggregates. Although feldspar was not analyzed, this textural disequilibrium is still reflected in minor but significant Sr-isotopic disequilibria between the other minerals (white mica, calcite/dolomite, and apatite) of this sample, resulting in an elevated MSWD of regression (Table 2). Nevertheless, a reasonably precise mylonitization age of 31.4 ± 0.9 Ma is calculated from the data (Fig. 10e). The age information is largely controlled by a fraction of large (250–160 μm) and particularly high-Rb/Sr mica crystals. White mica in this sample is Mg-rich, high-Si phengite with a remarkably uniform chemical composition with Si between 6.91 and 7.08 apfu (Table S1). Particularly large crystals of white mica are intimately intergrown with phlogopite. It is likely that the 250–160-μm white-mica crystal fraction had a significant phlogopite component in it, which would explain the high Rb/Sr ratio for this mica fraction. The microscopically observed unimodal grain-size distribution of the white-mica/phlogopite population, combined with the compositional homogeneity of both white mica and phlogopite (Table S1) indicates that the age of 31.4 ± 0.9 Ma reliably dates cessation of shearing in the rock.

The Rb—Sr mineral data for sample Su13–5 (lowermost Suretta nappe directly above Splügen zone, top-E kinematics) is characterized by small but significant Sr-isotopic disequilibria, both within the white-mica population and between the low-Rb/Sr phases albite and apatite (Fig. 10f). It is notable that the largest grain-size fraction of white mica (250–160 μm) plots slightly below the regression line for all data. This uncommon observation probably corresponds to the microscopic observation of particularly large white-mica crystals within texturally late shear bands. In electron backscatter imagery, no compositional zoning of white mica crystals is observed (Fig. 6d). The chemical composition of the white-mica population is homogeneous, with Si apfu between 6.65 and 6.81, in conjunction with an equally homogeneous Fe/(Fe + Mg) ratio around 0.38 (Table S1). Formally, an apparent age of 32.6 ± 0.5 Ma is calculated for the albite+white mica (250–160 μm) subassemblage. However, it remains unclear whether these two mineral subsamples really were in isotopic equilibrium at that time, and we prefer to stick to the higher uncertainty, but more reliable age estimate of 35.1 ± 4.2 Ma calculated from all mineral data of this sample as the best estimate for the timing of late stages of ductile deformation. Chemical homogeneity of the white-mica population with respect to major elements, combined with slight isotopic disequilibria may indicate a protracted deformation history.

Sample Su13–3 (lowermost Suretta nappe directly above Splügen zone, top-E kinematics) is a mylonite with conspicuous large feldspar (albite and K-feldspar) porphyroclasts. This pre-deformation feldspar fabric is reflected in Sr-isotopic disequilibrium between feldspar and epidote. Epidote is, in the same way as white mica, part of the fine-grained, fully recrystallized mylonitic subassemblage. Epidote also occurs intergrown with the mylonitic fabric-defining white-mica crystals.

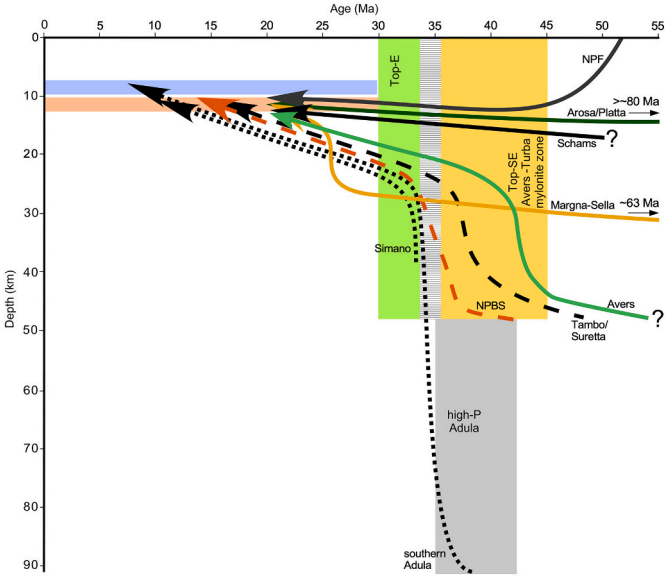


**Fig. 11.** Depth-time (P-t) diagram highlighting the significance of the Rb—Sr ages for the tectonic interpretation. The Arosa/Platta and Schams nappes show a flat exhumation path. The Avers Bündnerschiefer and the Suretta/Tambo nappes show distinct decompression at some stage after their high-P overprint — we show decompression as being caused by the Avers-Turba mylonite zone. The final exhumation of the Marnga-Sella nappe is due to movement on the Corvatsch detachment fault (Price et al., 2018). The Vals Bündnerschiefer and Adula nappe were mainly exhumed by top-E normal shearing. The vertical columns show the ages for the Avers-Turba mylonite zone (yellow) and top-E normal shearing (green); the hatched pattern marks where the ages for both deformation zones are grading into each other. The high-P overprint of Adula nappe (shown in grey) overlaps with the hatched and yellow patterns but the exhumation of the Adula nappe appears to be controlled by top-E normal shearing. The ZFT and ZHe ages have been converted to depths using a thermal gradient of 22°/km. (For interpretation of the references to colour in this figure legend, the reader is referred to the web version of this article.)

White mica has a homogeneous phengitic composition (Si between 6.77 and 6.93 apfu) with no indications for chemical zoning, and a homogeneous Fe/(Fe + Mg) ratio near 0.60 (Table S1). We therefore interpret the age of 34.3 ± 0.4 Ma obtained for epidote and two grain-size fractions of white mica (Fig. 10e) as accurately dating late stages of ductile deformation in this sample. The K-feldspar porphyroclast population appears to significantly predate the late deformation stages. However, the geological significance of the apparent age calculated for K-feldspar and white mica (39.1 ± 0.5 Ma) remains unclear.

Sample Su13–7 (uppermost Suretta nappe, cover, top-E kinematics) shows a very good though not perfect linear correlation of Rb—Sr mineral data for white mica, titanite and apatite corresponding to an age of 31.8 ± 1.5 Ma (Fig. 10g). Albite has not been analyzed as it is very rare in the rock and partly forms porphyroclasts. It appears that the largest grain-size white-mica population (>160 μm) of this fine-grained mylonite plots slightly above the regression line, although there is no clear microscopic evidence for textural disequilibria within the white-mica population in the rock. However, the chemical composition of white mica indicates that two groups of white mica may be distinguished, one with Si contents between 6.47 and 6.58 apfu and Fe/(Fe + Mg) near 0.57, in slight but significant contrast to a second group with Si contents <6.42 apfu and Fe/(Fe + Mg) >0.6 (Table S1). The latter group occurs preferentially within fine-grained domains within white-mica/chlorite-rich late shear bands (Fig. 6a), indicating that this may be a late white-mica generation formed during decompression. We therefore argue that the 31.8 ± 1.5 Ma age is a robust estimate for late stages of mylonitization, with an age uncertainty covering a somewhat prolonged history of waning of ductile deformation.

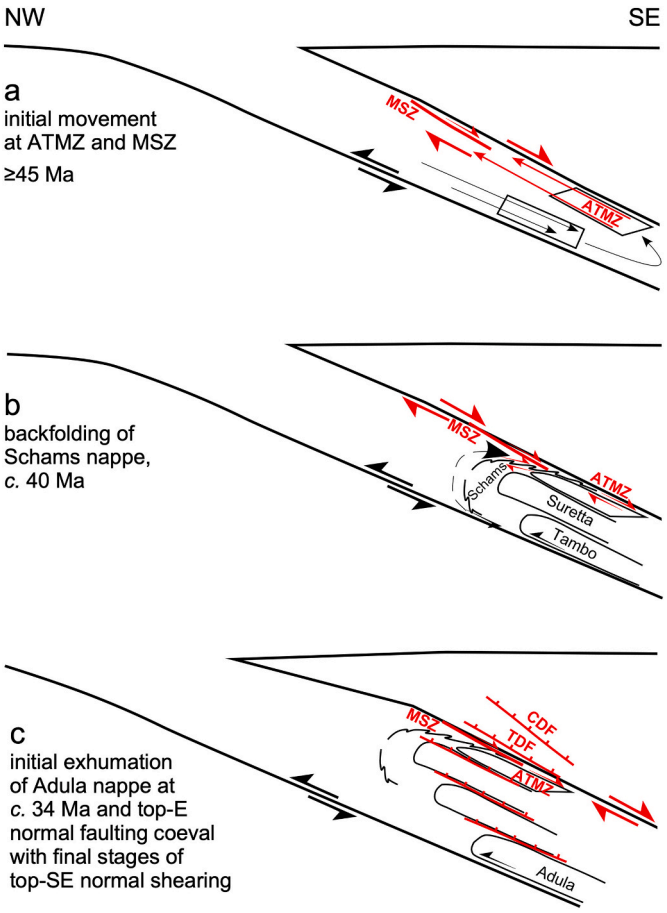


**Fig. 12.** Tectonic interpretation. (a) Pattern of return flow in subduction channel showing schematically the exhumation of the Avers Bündnerschiefer. Due to drag directly above the subduction thrust and underneath the overriding plate a velocity profile might result in which the more central parts of the subduction channel exhume faster. The Avers-Turba mylonite zone (ATMZ) develops because of this velocity profile. (b) The Schams nappe is wrapped around Tambo and Suretta fronts and caught up in a top-NW shear zone at base and a top-SE normal shear zone at the top. Note that we envisage the Martegnas shear zone (MSZ) as an upper-crustal fault associated with top-SE backflow in the Avers-Turba mylonite zone. (c) The main activity on the top-E structures is associated with initial thrusting and exhumation of the Adula nappe. TDF = Turba detachment fault, CDF = Corvatsch detachment fault.

### 6.4. Summary

The oldest age for ductile top-SE shearing is around 45 Ma from the Turba mylonite zone and the waning stages of top-SE shearing in the Avers and Turba mylonite zones are between 45 and 34 Ma (maximum 2σ uncertainty for the end of mylonitic shearing of samples Be14–12, Be14–13 and Su13–8). A recently reported $^{40}Ar/^{39}Ar$ white-mica age of 37.7 ± 1.1 Ma and a ZFT age of 35.5 ± 5.8 Ma from the Turba mylonite zone by Price et al. (2018) fit well with this age range. The latter two ages are interpreted to date mylonitic shearing and associated rapid cooling through the brittle-ductile transition zone. Our summary of the ages for Be14–12, Be14–13 and Su13–8, together with the consistent top-SE kinematic indicators, suggests that the Avers and the Turba mylonite zones are one and the same shear zone, the Avers-Turba mylonite zone. The age of 43.1 ± 1.4 Ma for sample Juf20-24 shows that the Martegnas shear zone moved at the same time as the Avers-Turba mylonite zone and both were active by about ≥45 Ma.

The Rb—Sr ages of the four samples from the zone of distributed top-E normal shearing above the Adula nappe range within 2σ uncertainty between >35 and 30 Ma. The older ages of 34.3 ± 0.4 Ma and 35.1 ± 4.2 Ma are both from the Splügen zone and are similar to the $^{40}Ar/^{39}Ar$ white-mica age of 35.7 ± 0.6 Ma reported by Challandes et al. (2003) (their sample is from close to our sample localities for Su13–3 and Su13–5) interpreted to date top-E shearing in the lower Suretta nappe.

Fig. 11 highlights the significance of the Rb—Sr ages in a depth-time (P-t) diagram. The non-high-P Arosa-Platta and Schams nappes (geothermal gradients ≥~20°C/km), as well as the North Pennine flysch show flat decompression paths. Movement in the Avers-Turba mylonite zone commenced before 45 Ma (note that the Rb—Sr ages date the cessation of mylonitization) and ceased by 40–34 Ma; hence, the Avers Bündnerschiefer have an early decompression phase starting at or before 45 Ma. The underlying Suretta and Tambo nappes, and the Vals Bündnerschiefer also show distinct decompression at some stage after their high-P overprint. We speculate that decompression was accomplished by both the Avers-Turba mylonite zone and distributed top-E normal shearing above the Adula nappe. For the Adula nappe, the coincidence in timing between top-E shearing and rapid cooling is strongly suggested by all available age data. Note that the ages of the Avers-Turba mylonite zone, distributed top-E normal shearing and high-P metamorphism of Adula nappe all are grading into each other at >35–34 Ma when the Adula nappe was initially being exhumed (Fig. 11).

## 7. Tectonic interpretation

We combine our structural and Rb—Sr data with published low-T thermochron ages and P-T data (Table 1) for a tectonic interpretation of the three P-breaks. Hence, our tectonic interpretation is based on a comprehensive data set but, as we will show, still remains speculative. We present our tectonic interpretation from old to young.

The first event is the high-P metamorphic overprint in the Avers Bündnerschiefer. Associated structures were overprinted by the Avers mylonite zone at ≥45–34 Ma. We have already suggested that the Turba and Avers mylonite zones are laterally continuous. The top-SE kinematic indicators in the upper parts of the Avers Bündnerschiefer in the Turba mylonite zone continue into the Avers shear zone further N, where the Turba mylonite zone cuts up section to the N. It is therefore conceivable that the Turba mylonite zone continues into the Avers shear zone and

both are one single structure, which we name the Avers-Turba mylonite zone. We regard the fault at the base of the Platta nappe with the cataclastic/brittle top-E kinematic indicators as a different structure and refer to it as the Turba detachment fault (see also below). This new classification helps to explain the disparate structural/kinematic data in the hanging- and footwall, and also the rather modest break in temperature of ~70° across the Turba mylonite zone as this modest break would now only be associated with the brittle Turba detachment fault.

Probably the simplest and most widely accepted interpretation would be to consider that the Avers-Turba mylonite zone formed, together with the contemporaneous Martgenas shear zone, due to return flow within the subduction channel and delimits the upper boundary of an extrusion wedge (cf., Ring and Glodny, 2010) (Fig. 12a). Gerya et al. (2002) numerically modelled this type of return flow and examples of subduction-related extrusion wedges exhuming high-P nappes have been proposed from other parts of the Alps (e.g., Eclogite zone (Glodny et al., 2008a) in the Tauern window and Combin shear zone (Reddy et al., 1999) in the Western Alps) and other Tethyian orogens (e.g., Argard et al. (2010) for the high-P belt in Oman, and Ring et al. (2020) from the Cycladic blueschist unit in the Aegean Sea region). If the return-flow hypothesis was accepted, the Avers-Turba mylonite zone would have started to form at ≥45 Ma and be related and succeeding high-P metamorphism of the Avers Bündnerschiefer as the dated top-SE mylonites contain high-Si phengite with rims having lower Si contents. An age of, say, ~50 Ma for high-P metamorphism in the Avers Bündnerschiefer would be in line with the final stages of thrusting of the mildly-high-P Margna nappe and the non-high-P Arosa and Platta units onto the underlying high-P units at 54.5–46.7 Ma (maximum 2σ uncertainty of deformation ages in Table 1). The Martegnas, and possibly also the Gürgaletsch shear zones are considered high-level normal shear zones that ultimately sole out in the Avers-Turba mylonite zone during progressive exhumation juxtaposing the non-high-P North Pennine flysch against the lower greenschist-facies Schams nappe and the deeper high-P nappes. The broad age range of ≥45–34 Ma for the blueschist/greenschist-facies (~400°C) Avers-Turba mylonite zone and the ZFT age of 35.5 ± 5.8 Ma (Price et al., 2018) (Table 1) allows to approximate a crude cooling rate of ~30°C/Ma for the Avers Bündnerschiefer. The ZFT age constrains the passage of the Avers Bündnerschiefer through the brittle-ductile transition zone and although the ZFT age has large errors it suggests exhumation rates of 2–6 km/Ma for the time interval between ≥45–34 and 35.5 ± 5.8 Ma for an approximately 15 km deep brittle-ductile transition.

Consistent with existing models (e.g., Schmid et al., 1996), we envisage that the Avers-Turba mylonite zone developed in the upper, backfolded limb of the Niemet-Beverin fold. Nievergelt et al. (1996) already speculated that the Turba mylonite zone might be as old as 45 Ma and related to the Niemet-Beverin backfolding phase. Above the Adula nappe, top-N/NW structures occur in the Misox zone and the overlying Schams nappe and are generally interpreted to be related to top-N/NW thrusting largely preceding but also accompanying backfolding (Schreurs, 1993; Pleuger et al., 2003). Hence, our ages of ≥45–34 Ma for the upper limb of the backfold should also be valid for top-N/NW thrusting in the lower limb of the Niemet-Beverin fold, although top-N/NW thrusting had already started earlier.

How does the Schams nappe get backfolded in the shallow parts of the extrusion zone at depths of about 15–20 km and P-break-1 being folded in a return flow scenario? We have argued above, that the upper contact of this backfold had to be normal to the Earth surface and cannot be a backthrust associated with the formation of the southern steep belt and the Insubric line. If backfolding at ≥45–34 Ma was envisaged for the formation of the Avers-Turba mylonite zone, then this would explain the folded structure of P-break-1. In the western, structurally lower segment, P-break-1 would have been created by thrusting of the exhuming Tambo/Suretta nappes onto the Schams nappe. Subsequently, the Schams nappe was wrapped around the Tambo/Suretta nappes and the upper backfolded parts of it were caught up in the top-SE Avers-Turba mylonite zone (Fig. 12b).

As mentioned above, the original proposition of the Niemet-Beverin backfold by Schmid et al. (1990) was inspired by the analogue models of Merle and Guillier (1989) and the backfolding process was mainly considered to have occurred when the backfolded nappe stack was already in a subhorizontal position, for which there is no support before ~20 Ma (Price et al., 2018, their fig. 17). The vertical velocity profile for the formation the Niemet-Beverin backfold explains the reversal in shear sense from the lower to the upper, inverted limb (cf. Schmid et al., 1990). In the subduction channel, this velocity profile postulates higher exhumation rates in the center of the exhuming nappe pile (Fig. 12b). The folding process would have been aided by a component of vertical shortening, i.e., general-shear deformation. Indications for general shear are the top-SE and top-NW kinematic indicators in the Avers-Turba mylonite zone as well as the flattening strain geometries reported by Ring (1992b) and Scheiber et al. (2012).

A remaining problem still is to identify the former basement of the Schams nappe. Schreurs (1993) suggested that it is probably represented by parts of the Tambo and/or Suretta basement nappes. However, that would mean that both nappes are inverted, which contradicts propositions that the lower parts of the Permo-Mesozoic sediments in the Splügen zone above the Tambo nappe are the autochthonous cover of the Tambo basement (Strobach, 1965; Blanc, 1965; Schreurs, 1993; Scheiber et al., 2012). It appears more likely that the basement of the Schams nappe is either the non-high-P Middle Pennine Maggia nappe further west (Figs. 1, 2), or it has been completely subducted.

Distributed, ductile top-E normal shearing occurred between >35 and 30 Ma and, within 2σ uncertainty, overlapped with the ≥45–34-Ma-old Avers-Turba mylonite zone at around 35–34 Ma. The oldest ages for top-E shearing of >35 Ma, and also the age of 35.7 ± 0.6 Ma of Challandes et al. (2003), are from the Splügen zone in a central part of the exhuming zone where velocities and velocity gradients might have been high. Therefore, rocks deformed earlier and retain older ages than in zones of smaller velocities above (sample Su13–7 (31.8 ± 1.5 Ma) from the Suretta cover) and below (sample Be14–7 (31.4 ± 0.9 Ma) from the Misox zone) the Splügen zone (Fig. 12b). A remaining fundamental problem is why normal shearing occurred in the *E*-W direction at a high angle to top-N/NW thrusting and top-SE normal backshearing? The earliest evidence for orogen-parallel E-W normal faulting is from the Tauern Window of the Eastern Alps at about 30 Ma (Glodny et al., 2008a; Favaro et al., 2015) and thus at a time when top-E normal shearing in the eastern Central Alps was about to end. We can only speculate that top-E shearing was guided by pre-existing anisotropies and/or an easterly dip of the top-W/NW thrust planes, i.e., that there was an angle between the direction of subduction and thrusting in the subduction channel (see also section 9.3. below).

Top-E normal shearing overlapped in time with top-SE normal shearing at about >35–34 Ma. It has been proposed that the E-W stretching lineations are parallel to the axes of the Niemet-Beverin backfold (Baudin et al., 1993; Marquer et al., 1996), although our data shown in Figs. 5, 8 and 9 suggest the stretching lineations are at a small but distinct angle to the Niemet-Beverin backfold axis (see also Ring, 1992b). The S-closing counterpart of the Niemet-Beverin fold is obscured by the Turba mylonite and detachment zones (Nievergelt et al., 1996) at the base of the Platta nappe. The structures of the top-E Turba detachment fault obliquely crosscut the Avers-Turba mylonite and Martegnas shear zone, and also nappe boundaries by cutting deeper into the nappe pile to the S (Fig. 12c). We envisage that the Turba detachment fault is a high-level, low-angle, normal fault associated with distributed, ductile top-E normal shearing above the Misox zone.

Ages of >35–30 Ma just overlap with the age of high-P metamorphism (~40–35 Ma) and initial exhumation of the Adula nappe at 34 Ma. Therefore, top-E normal shearing created P-break-3 and aided the exhumation of the Adula nappe by reducing its overburden as the Adula nappe was emplaced above the underlying distinctly lower-P Simano and Leventina nappes by top-N/NW thrusting (Rütti, 2003).

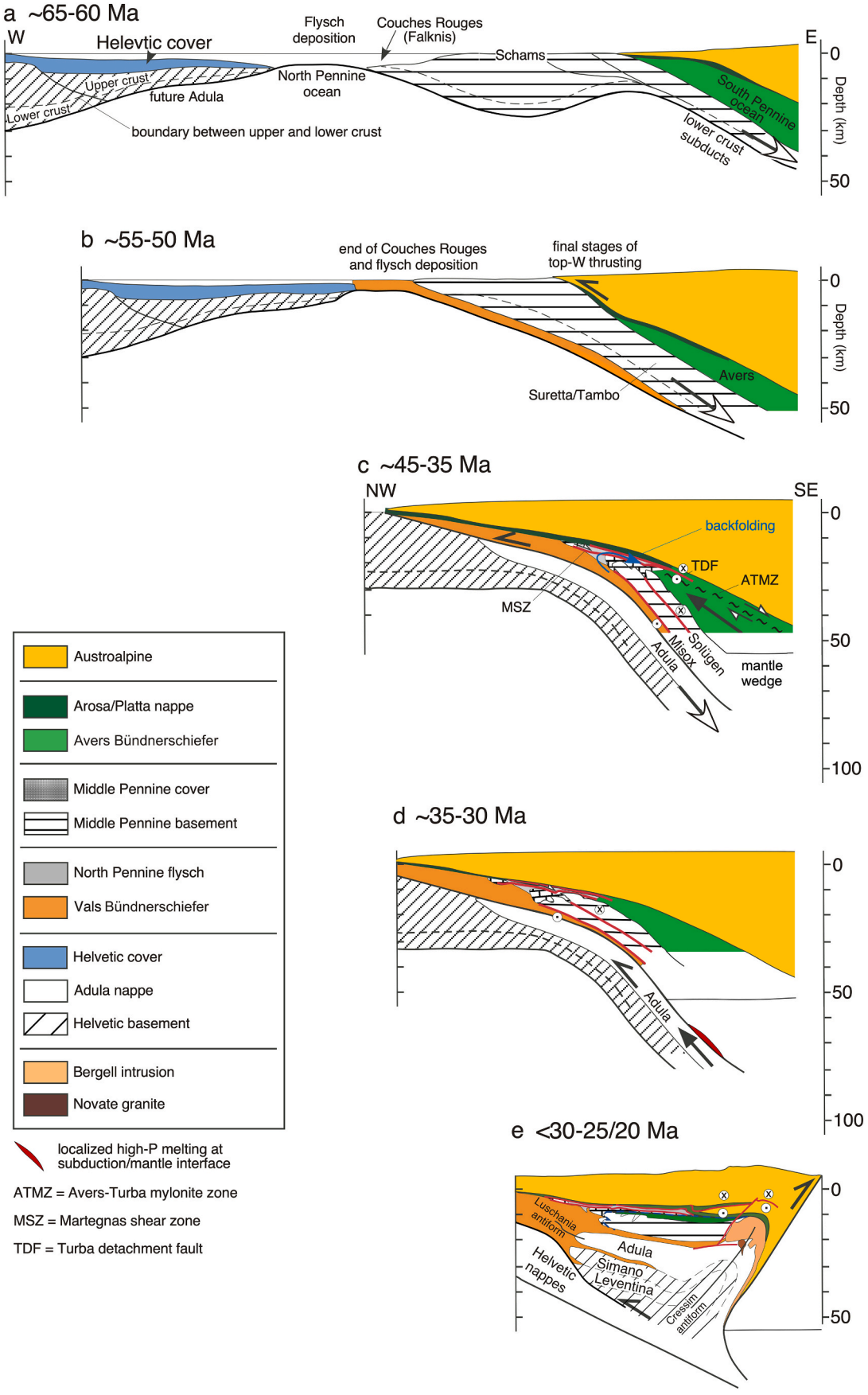


*(caption on next page)*

**Fig. 13.** Tectonic history. Sketches highlighting our interpretation of the tectonic evolution of eastern Central Alps. Note that the sketches intentionally resemble those of Schmid et al. (1996) and are modified to account for our new and other published data (Price et al., 2018), which are, in part, at variance with the Schmid et al. model. The subduction geometry is according to Doglioni et al. (1999) mimicking an advancing plate boundary. (a) Situation at the Cretaceous/Tertiary boundary when the Austroalpine Margna-Sella nappe, the Arosa zone and the Platta nappe were still being thrust westward closing the South Pennine ocean. (b) At ~55–50 Ma, the Margna-Sella nappe and the Arosa zone were in the final stages of top-W imbrication and sedimentation of the Middle Pennine Couches Rouges and the North Pennine flysch ceased by ~52 Ma. From now on deposition in the Central Alps transect was restricted to the foredeeps (Molasse basin and Po Plain in Fig. 1). (c) At ≥45 Ma the Avers-Turba mylonite zone (ATMZ) formed and the Schams nappe was subsequently caught up below the exhuming Tambo nappe at 15–20 km depth and started wrapping around the Tambo and Suretta front. The Adula nappe reached maximum depth and its high-P overprint. MSZ = Martegnas shear zone, TDF = Turba detachment fault. (d) The main event at 35–30 Ma was the thrusting of the Adula nappe onto the underlying nappes and pronounced top-E normal shearing above the Adula nappe. Note high-P melting of eclogite at the interface between the subducting slab and the overlying mantle wedge (Pellegrino et al., 2020). (e) At ~32–30 Ma the Bergell pluton intruded and strong S-directed backshearing formed the southern steep belt between ~30 and 25/23 Ma. At the end of this time window tangential extension affected the Central Alps. See text for more explanation.

The latter two nappes also show a N-S P-T gradient and the pressure gap between those nappes and the Adula nappe is of the order of 11–14 kbar (equaling 40–50 km of structural section). During thrusting, the Adula nappe experienced exhumation rates >15 km/Ma demanding that normal shearing above the Adula nappe that largely aided the exhumation must have also been rapid.

What about P-break-2? We suggest that P-break-2 formed at about the same time as P-break-3 separating the high-P Vals Bünderschiefer from the overlying Schams nappe and North Pennine flysch by ductile top-E normal shearing. The ages of initial exhumation of the Vals Bündnerschiefer and the Adula nappe are ~34 Ma (Hermann et al., 2006; Wiederkehr et al., 2009). Arguably P-break-2 is also affected by the northernmost trace of the Niemet-Beverin fold (Weh and Froitzheim, 2001) (Fig. 2). However, our field data do not allow us to further discuss the role of P-break-2 NE of the Misox zone.

All P-breaks converge in the Misox zone, which is the root zone of the Vals Bündnerschiefer and the suture zone between the European margin and the Briançonnais microcontinent (Fig. 2). We envisage that the pronounced thinning of the Misox zone is a combined effect of early top-N/NW general-shear thrusting (cf., Kassem and Ring, 2004; Ring and Kassem, 2007) and ensuing top-E general-shear normal movement above the Adula nappe. Both events had a component of vertical ductile thinning. Further S, the Misox zone is cut out by the top-NE Forcola normal fault.

Possible displacements for the various normal shear zones and faults can be approximated. The Avers-Turba mylonite zone exhumed the Avers Bündnerschiefer from about 50 km depth and juxtaposed it together with the Martegnas shear zone against the North Pennine flysch for which a maximum depth of about 15 km can be derived from the P-T data (Figs. 4, 11). Assuming a 45°-dipping subduction channel (Price et al., 2018) results in a displacement of ~50 km for the Avers-Turba mylonite zone and Martegnas shear zone. Most of this displacement would have been taken up by the Avers-Turba mylonite zone. If the P-T data of Baudin and Marquer (1993) for decompression of the Tambo nappe are also valid for the Suretta nappe and its cover, and a 30° dip for the top-E shear zones is considered, a displacement of 75 km results. These figures are in agreement with the 60 km of minimum top-to-the-S/SE displacement proposed by Price et al. (2018). Note that Price et al. (2018) argued that the preserved N-S structural overlap between Austroalpine and Penninic units of 70 km is a minimum amount of displacement. The exhumation caused by top-SE and top-E normal shearing would be of the order of 70 km. This estimate is likely too high as both processes overlapped in time and top-E normal shearing contributed to thinning below the Avers-Turba mylonite zone. Nonetheless, the figures show that normal movement on those two structures can largely account for the missing crust between the Adula nappe and the non-high-P units below the Pennine-Austroalpine boundary zone.

How was the 70 km of N-S overlap reported by Price et al. (2018) accomplished? The displacements we approximated are from the top-SE Avers-Turba mylonite zone and distributed top-E normal shearing and both have a distinct easterly component. Top-E normal shearing does not contribute to the 70 km of N-S overlap. The southerly component of motion of the Avers-Turba mylonite zone would be almost 40 km. We would need to conclude that the top-SE Martegnas shear zone and the top-SSE Gürgaletsch shear zone account for the remaining ~30 km of 'missing' structural overlap. Because both shear zones hardly cut out any metamorphic section, their dip angles must have been very low. Such a scenario would explain that the Martegnas shear zone brought the North Penninic flysch into its southern position (Fig. 2). However, these estimates depend on the exact azimuth of 'N-S'. If this azimuth was, say, 340°, then top-SE and top-E normal shearing had indeed contributed ~70 km to the NNW-SSE overlap.

## 8. Tectonic history

In Fig. 13 we show sketches based on Schmid et al. (1996) illustrating our interpretation of the tectonic history of Central Alps. We start near the Cretaceous/Tertiary boundary (Fig. 13a). At this stage the 'orogenic lid' was still being thrust westward, the South Pennine ocean was closed and sedimentation in the Schams nappe had ceased (Schmid et al., 1990; Schreurs, 1993). Nonetheless, further NW in the Middle Pennine realm, deep-pelagic marls (Couches Rouges) were still being deposited as recorded in the Falknis nappe, and the North Pennine ocean continued to receive flysch sediments. This sedimentation pattern with deep marine marls forming closer to the advancing thrust front than the flysch appears unusual. A probable scenario would be a strike-slip margin as already suggested by Ring et al. (1989) and Ring (1992b, 1994) associated with top-W thrusting. Carminati and Doglioni (2012) considered this strike-slip margin in the Central and Eastern Alps the transpressive part of the Cretaceous/early Cenozoic Alpine orogen (emphasizing that convergence in the Alps was distinctly oblique).

At ~55–50 Ma, the Margna nappe and the Arosa zone were in the final stages of top-W imbrication and the Avers Bündnerschiefer may have experienced their high-P overprint (or earlier), the Suretta and Tambo were being underthrust or already underplated (Fig. 13b). The deposition of the North Pennine flysch ceased by ~52 Ma, probably due to initial collision of the Middle Pennine microcontinent with the European margin. We show *E*-W cross sections for the first two steps until ~50 Ma (Fig. 13a, b), which is complementary to Schmid et al. (1996), who showed N-S cross sections. However, there are no data supporting N-S nappe transport before ~50 Ma (Ring et al., 1988, 1989; Platt et al., 1989; Schmid and Hass, 1989; Biehler, 1990; Liniger, 1992; Dürr, 1992; Handy et al., 1996).

At ≥45–34 Ma, shearing in the Avers-Turba mylonite zone and the Martegnas shear zone was underway and strongly aided the exhumation of the Avers Bündnerschiefer, and possibly also the Suretta and Tambo nappes (Fig. 13c). The Schams nappe got caught up beneath and in front of the exhuming Tambo nappe at 15–20 km depth and started wrapping around the Tambo and Suretta fronts. At >35 Ma distributed top-E normal shearing below the Avers-Turba mylonite zone overlapped in time with the latter. The final stages of high-P metamorphism in the Adula nappe occurred during this stage. The main event at 35–30 Ma was the thrusting of the Adula nappe onto the Simano and Leventina nappes coeval with pronounced top-E normal shearing above the Adula nappe. Pronounced normal faulting above the Adula nappe was necessary to remove its overburden for explaining P of 'only' ~10 kbar in the

nappes below the Adula nappe. Incipient exhumation of the Adula nappe at 34.2 ± 0.2 Ma (Hermann et al., 2006) caused eclogite melting that interacted with garnet peridotite of the supra-subduction mantle (Pellegrino et al., 2020). The ages for ultrahigh-T metamorphism in the Gruf complex and the amphibolite-facies overprint of the southern Adula nappe (33.4–30.9 Ma), are slightly older but overlap with the Bergell tonalite intrusion (32–31.1 Ma). Late during this stage, the Bergell granodiorite intruded at ~30 Ma (von Blanckenburg, 1992; Oberli et al., 2004). We consider it likely that eclogite melting at the subduction zone/mantle interface at or after 34.2 ± 0.2 Ma resulted in the intrusion of the Bergell tonalite and granodiorite, and is causally related to the (ultra)high-T overprint (Fig. 13d).

Strong S-directed backshearing/thrusting formed the southern steep belt between ~30 and 25/23 Ma. During this time, tangential stretching affected the Central Alps and caused *E*-W extension and normal faulting at the Forcola, Muretto and Engadine faults occurred. The Corvatsch detachment fault, and maybe also the Turba detachment fault, may have moved at this stage as well, as suggested by low-T thermochronology (Price et al., 2018).

For the stages between 45 and 25/20 Ma (Fig. 13c–e) we propose a pronounced component of top-SE normal shearing and also important E-W tangential normal shearing, which is at variance with the traditional Schmid et al. (1996) model. However, our results confirm Price et al. (2018) arguing that the dominant kinematic slip vector is E to SE.

We have argued that backfolding and the formation of the top-SE Avers-Turba mylonite zone and the associated Martegnas and Gürgaletsch normal shear zones were unrelated to the formation of the southern steep and the Insubric line. Crosscutting relations indicate that top-SE backshearing/backthrusting at the Insubric line commenced after 32 Ma. The ~32 Ma Bergell tonalite and its contact with the Gruf complex show upright folds resulting from N-S shortening and magma intruded along the fold axes (Rosenberg et al., 1995; Davidson et al., 1996). The onset of rapid erosion of the Bergell intrusion at ~25 Ma (Malusà et al., 2011) and N—S tilting of the pluton between ~25 and 16 Ma (Garzanti and Malusà, 2008) suggests that top-SE backshearing/backthrusting commenced by about 25 Ma.

## 9. Discussion

We discuss whether normal shearing/faulting occurred during lithospheric shortening or lithospheric extension. We especially compare our results with the ZFT and ZHe data of Price et al. (2018), the latter of which relate to shallower phases of movement than our Rb—Sr mylonite ages constraining earlier tectonic stages in part coeval with high-P metamorphism.

### 9.1. Normal shearing during lithospheric shortening

We argued that normal shearing at the ≥45–34 Ma Turba-Avers mylonite and Martegnas shear zones, as well as distributed, ductile top-E shearing below it cannot be due to crustal extension as envisaged by Baudin and Marquer (1993), Nievergelt et al. (1996), Weh and Froitzheim (2001) and Beltrando et al. (2010) as normal shearing needs to be associated with thrusting in deeper units at the same time to explain (ultra)high-P in Adula nappe at ~40–35 Ma. Likewise, normal shearing needs to have reduced the overburden of the Adula nappe while the latter was thrust onto the non-high-P Simano and Leventina nappes starting at ~34 Ma. This thrusting excised 40–50 km of section, which translates into a thrust displacement of 55–70 km for a 45°-dipping subduction zone. Above we suggested that top-E normal shearing accounts for a displacement of 75 km, which basically matches the thrust displacement below the Adula nappe. Our arguments show a coeval and close relationship between large-scale lithospheric shortening and crustal-scale normal shearing.

The envisaged extrusion wedge interpretation highlights that large-scale normal faulting occurred coevally with thickening. Such a conclusion has already been proposed by Price et al. (2018). The latter authors regard the Pennine domain as a large-scale extrusion wedge or 'mega-pip' (cf., Wheeler et al., 2001) between about 50–29 (possibly 18) Ma and argued that the geometry of the 'mega-pip' can explain many of the enigmatic features found at the top of the Pennine zone, including the southerly position of the North Pennine flysch, the apparent south vergence of the Schams nappe over the Avers Bündnerschiefer and the backfolded 'fingers' at the top of the Suretta nappe (Fig. 3). We believe that a return-flow model best explains the piecemeal exhumation of the nappes from top to bottom in the eastern Central Alps. Gerya et al. (2002) numerically modelled such return flow in the subduction channel using low-viscosity rheologies of the extruding material. Such a scenario may simulate the extrusion of Avers Bündnerschiefer but probably not that of the Adula, Tambo and Suretta basement nappes (see for instance restoration by Price et al. (2018) of coherent Pennine/distal Helvetic slab). We suggest that return flow affected these basement nappes as rather coherent nappes. These nappes underwent internal ductile deformation but did not behave as low-viscosity bodies. Note that return flow may have been aided by buoyancy forces and both processes are not mutually exclusive.

Malusà et al. (2015) argued that subduction-channel return flow requires a stationary wedge and fixed boundaries within the subduction zone, and that the top of the extruding material needs to be constantly removed (trimmed back) by erosion, requiring the generation of large amounts of syn-exhumation sediment. Malusà et al. (2015) claimed that these large amounts of sediment do not exist in the Western Alps. However, they acknowledge that the Oligo-Miocene sediments in the Northern Apennines S of the Po Plain (Fig. 1) reflect considerable volumes of eroded material from the Central Alps (Di Giulio, 1999; Di Giulio et al., 2001). As shown by Ring and Yngwe (2018), material at the front of an extruding high-P wedge in Crete (Hellenic subduction zone in the eastern Mediterranean) was laterally removed by out-of-sequence thrusts. In other words, large amounts of erosion are not needed if the front of an extruding wedge was trimmed back tectonically. Furthermore, a stationary wedge with fixed boundaries is probably not a plausible scenario for the evolving Alps in the Tertiary where material from the down-going plate was gradually accreted and the deformation front shifted towards the foreland.

Price et al. (2018) argued that buoyancy forces due to deep subduction of the Adula nappe into the lithospheric mantle triggered exhumation and largely guided tectonic processes in the Central Alps subduction channel. Because all ages (Avers-Turba mylonite zone at ≥45–34 Ma, distributed top-E shearing at >35–30 Ma and high-P in the Adula nappe at ~40–35 Ma) are grading into each other around 35 Ma, it appears conceivable that deep exhumation of the Adula nappe may indeed have had an important effect on tectonic processes in the Central Alps. However, the initial exhumation of the Adula nappe commenced at about 34 Ma (Hermann et al., 2006) and the youngest permissible age of sample Be14–13 from the Avers-Turba mylonite zone is 38.7 Ma and thus almost 5 Ma older than deep exhumation of the Adula nappe. There is a spatial direction of the isotopic ages progressing from tectonic top to bottom. Although activity intervals of tectonic processes might glide into each other they are chronologically distinct (e.g., Fig. 13c, d). Nonetheless, proponents of buoyancy-driven exhumation models may argue that the oldest permissible age for high-P metamorphism in the Adula nappe is around 45 Ma (43.9 ± 5.7 Ma age of Becker, 1993) and provided the buoyancy to drive the 'mega-pip' since ~45 Ma.

### 9.2. Tangential extension and normal faulting

Price et al. (2018) claimed that the large component of top-S/SE net motion was at a high angle to the overall E-W trend of the Alps at this longitude and is therefore kinematically distinct from, and earlier than, Miocene orogen-parallel (tangential) crustal extension. The absence of any extensional sedimentary basins associated with tangential extension in the eastern Central Alps makes it hard to put tight constraints on the

start of this process. The cause for tangential (E-W) extension in the Central Alps might have been the rotation of the Western Alps, whereas in the Eastern Alps it is related to eastward escape in the Tauern Window and east of it (Ratschbacher et al., 1991). The main structure accommodating rotation of the Western Alps and E-W extension is the Simplon line in the hinge zone between the Western and Central Alps (Fig. 1). Horizontal extension across the Simplon line is ~16 km (Steck, 1984; Mancktelow, 1990). Steck and Hunziker (1994) inferred that faulting and thus E-W extension commenced at 25 Ma, while Campani et al. (2010) suggested that the shear zone was at least active since 20 Ma. The probably best estimate for the onset of E-W extension in the eastern Central Alps are U—Pb calcite ages of 25.3 ± 5.6 to 21.8 ± 3.4 Ma (Ring and Gerdes, 2016) from the V-shaped Alpine Rhinegraben (Fig. 1).

The brief summary of the timing of E-W extension in the Central Alps shows that the main phases of movement we constrained for the Avers-Turba mylonite zone and ductile top-E normal shearing cannot be due to orogen-parallel E-W extension. However, the low-T thermochron ages of Price et al. (2018) show final normal movements after about 25 Ma (which we take as a proxy for the initiation of tangential extension). Movement on the top-E Corvatsch detachment ceased by 25 Ma (fig. 15 in Price et al., 2018). We envisage it likely that final increments of slip at the other top-E/NE normal faults also occurred at and after 25 Ma and thus were caused by orogen-parallel extension. NE-directed normal faulting at the Forcola and Muretto faults are also due to tangential stretching after ~25 Ma (Ring, 1994b; Ciancaleoni and Marquer, 2008). The total amount of E-W extension is modest indicating that horizontal E-W extension did not play an important role in the Central Alps.

### 9.3. Implication for tectonic models

We have shown that late Eocene to early Oligocene top-E normal shearing during lithospheric shortening accounts for ~75 km displacement and Miocene top-E crustal extension for much less E-W extension. There is also a large component to top-SE normal shearing. Overall, the large component of tangential movements demonstrates that mountain building in the Alps is an inherently three-dimensional process. Consequently, crosscutting relations of the Bergell pluton do not rigorously show that nappe-stacking processes in the Alps were completed by 32–30 Ma, as demonstrated for instance by eclogite-facies metamorphism and subsequent emplacement of the eclogite zone in the Tauern Window of the Eastern Alps at 32–30 Ma (Glodny et al., 2005, 2008a). Thus, cylindrical two-dimensional tectonic models are problematic.

The Butler et al. (2013) numerical model simulating exhumation processes in the Western Alps produced localized orthogonal extension in the upper crust accommodating the exhumation of extruding wedges. Malusà et al. (2015) also envisaged extension aiding deep exhumation due to the upper plate moving away from the trench. In the Central Alps there is no evidence for any horizontal extension between 45 and 25 Ma. However, most upper crustal rocks are eroded, so evidence for localized upper-crustal extension may have been erased. The distinct three-dimensional aspects we have demonstrated make 'orthogonal' extension as inferred from two-dimensional modeling difficult to apply to the Alps.

While the tectonic models of Schmid et al. (1996), Rosenberg and Kissling (2013) and the numerical simulation of Butler et al. (2013) are two dimensional, Carminati and Doglioni (2012) considered the Cretaceous and early Cenozoic Alps a three-dimensional transpressive orogen above an E-dipping subduction zone in which the subduction hinge converged relative to the overriding Adriatic Plate (Doglioni et al., 1999). Malusà et al. (2015) also envisaged a distinctly three-dimensional geometry of Alpine convergence. This proposition offers a possibility to better understand why large-scale, non-extensional tangential motion was an integral part of the Eocene/Oligocene orogeny in the Central Alps. Pre-existing anisotropies from Cretaceous/early Tertiary E/SE-directed subduction and associated top-W thrusting may have guided top-E motion along inherited discontinuities.

## 10. Conclusions

We have defined three major breaks in metamorphic pressure across the nappe pile of the eastern Central Alps and argued that the P-breaks were caused by major normal shearing coeval with lithospheric shortening in the Alpine subduction channel. We correlate the top-SE Avers shear zone with the Turba mylonite zone and constrained mylonitization to ≥45–34 Ma. Movement in the Avers-Turba mylonite zone overlapped in time with distributed top-E normal shearing above the ultrahigh-P Adula nappe. Top-E normal shearing took place between >35–30 Ma. Both normal shearing events removed the overburden of the Adula nappe explaining why the nappes below the Adula nappe do not have a high-P overprint. After about 25 Ma there was modest E-W extension in the Central Alps. Overall, our data show considerable out-of-plane movements and are not compatible with simple, sustained top-N/NW thrusting as traditionally envisaged. A major conclusion is that our data indicate considerable tangential out-of-plane movements during overall top-N/NW thrust propagation in the Central Alps rendering two-dimensional tectonic models problematic and show that mountain building in the Alps was an inherently three-dimensional process. Our work shows that quantitative, field-based data sets combining structural data, P-T estimates and geochronology are most essential assets for understanding orogenic deformation.

Supplementary data to this article can be found online at https://doi.org/10.1016/j.earscirev.2021.103644.

## Declaration of Competing Interest

The authors declare that they have no known competing financial interests or personal relationships that could have appeared to influence the work reported in this paper.

## Acknowledgements

This work has been supported by funds from Stockholm University. Reuben Hansman provided an informal review and Kurt Decker helped with the Rhenodanubian flysch. O. Appelt and F. Wilke helped with electron microprobe work at GFZ Potsdam, which is gratefully acknowledged. We thank two anonymous reviewers and editor Carlo Doglioni for comments that helped to improve the manuscript.

## References

Allemann, F., 1952. Die Couches Rouges der Sulzfluhdecke im Fürstentum Liechtenstein. Eclogae Geol. Helv. 45, 294–298.
Argand, É., 1916. Sur l'arc des Alpes Occidentales. Eclogae Geol. Helv. 14, 145–191.
Argard, P., Searle, M.P., Alsop, G.I., Dubacq, B., B., 2010. Crustal stacking and expulsion tectonics during continental subduction: P-T deformation constraints from Oman. Tectonics 29, TC5018. https://doi.org/10.1029/2010TC002669.
Bachmann, R., Glodny, J., Oncken, O., Seifert, W., 2009. Abandonment of the South Penninic–Austroalpine palaeosubduction zone, Central Alps, and shift from subduction erosion to accretion: constraints from Rb/Sr geochronology. J. Geol. Soc. 166, 217–231.
Baudin, T., Marquer, D., 1993. Métamorphisme et déformation dans la nappe de Tambo (Alpes centrales suisses): évolution de la substitution phengitique au cours de la déformation alpine. Schweiz. Mineral. Petrogr. Mitt. 73, 285–299.
Baudin, T., Marquer, D., Persoz, F., 1993. Basement-cover relationships in the Tambo nappe (Central Alps, Switzerland): geometry, structures and kinematics. J. Struct. Geol. 15 (3–5), 543–553.
Becker, H., 1993. Garnet peridotite and eclogite Sm–Nd mineral ages from the Lepontine dome (Swiss Alps): new evidence for Eocene high-pressure metamorphism in the Central Alps. Geology 21, 599–602.
Beltrando, M., Lister, G.S., Rosenbaum, G., Richards, S., Forster, M.A., 2010. Recognizing episodic lithospheric thinning along a convergent plate margin: the example of the early Oligocene Alps. Earth Sci. Rev. 103, 81–98. https://doi.org/10.1016/j.earscirev.2010.09.001.
Bender, H., Ring, U., Almqvist, B.S.G., Grasemann, B., Stephens, M.B., 2018. Metamorphic zonation by out-of-sequence thrusting at back-stepping subduction zones: Sequential accretion of the Caledonian internides, Central Sweden. Tectonics 37, 3545–3576. https://doi.org/10.1029/2018TC005088.

Biehler, D., 1990. Strukturelle Entwicklung der Penninisch-Ostalpinen Grenzzone am Beispiel der Arosa Zone im Ost-Rätikon (Vorarlberg, Österreich). Eclogae Geol. Helv. 83, 221–239.
Blanc, B.L., 1965. Zur Geologie zwischen Madesimo und Chiavenna. Mitt. geol. Inst., ETH und Univ, Zurich [N.F.], p. 57.
Bousquet, R., Goffé, B., Vidal, O., Oberhansli, R., Patriat, M., 2002. The tectono-metamorphic history of the Valaisan domain from the Western to the Central Alps: new constraints on the evolution of the Alps. GSA Bull. 114 (2), 201–225.
Boutelier, D., Chemenda, A., Jorand, C., 2004. Continental subduction and exhumation of high-pressure rocks: insights from thermomechanical laboratory modeling. Earth Planet. Sci. Lett. 222, 209–216.
Brouwer, F.M., Burri, T., Engi, M., Berger, A., 2005. Eclogite relics in the Central Alps: PT-evolution, Lu-Hf ages, and implications for formation of tectonic melange zones. Schweiz. Mineral. Petrogr. Mitt. 85, 147–174.
Butler, J.P., Beaumont, C., Jamieson, R.A., 2013. The Alps 1: a working geodynamic model for burial and exhumation of (ultra)high-pressure rocks in Alpine-type orogens. Earth Planet. Sci. Lett. 377-378, 114–131.
Campani, M., Mancktelow, N., Seward, D., Rolland, Y., Müller, W., Guerra, I., 2010. Geochronological evidence for continuous exhumation through the ductile–brittle transition along a crustal-scale low-angle normal fault: simplon Fault Zone, Central Alps. Tectonics 29, 1–25.
Carminati, E., Doglioni, C., 2012. Alps vs. Apennines: the paradigm of a tectonically asymmetric Earth. Earth Sci. Rev. 112, 67–96. https://doi.org/10.1016/j.earscirev.2012.02.004.
Challandes, N., Marquer, D., Villa, I.M., 2003. Dating the evolution of C-S microstructures: a combined $^{40}Ar/^{39}Ar$ step-heating and UV laserprobe analysis of the Alpine Roffna shear zone. Chem. Geol. 197, 3–19.
Choukroune, P., Ballèvre Cobbold, P., Gautier, Y., Merle, O., Vuichard, J.P., 1986. Deformation and motion in the Western Alpine Arc. Tectonics 5. https://doi.org/10.1029/TC005i002p00215.
Ciancaleoni, L., Marquer, D., 2008. Late Oligocene to early Miocene lateral extrusion at the eastern border of the Lepontine Dome of the Central Alps (Bergell and Insubric areas, eastern Central Alps). Tectonics 27, TC4008. https://doi.org/10.1029/2007TC002196.
Dale, J., Holland, T.J.B., 2003. Geothermobarometry, P-T paths and metamorphic field gradients of high pressure rocks in the Adula Nappe, Central Alps. J. Metamorph. Geol. 21, 813–829.
Davidson, C., Rosenberg, C., Schmid, S.M., 1996. Synmagmatic folding of the base of the Bergell pluton, Central Alps. Tectonophysics 265, 213–238.
Dewey, J.F., Helman, M.L., Turco, E., Hutton, D.W.H., Knott, S.D., 1989. Kinematics of the western Mediterranean. In: Coward, M.P., Dietrich, D., Park, R.G. (Eds.), Alpine Tectonics, 45. Spec. Publs Geol. Soc. Lond, pp. 265–283.
Di Giulio, A., 1999. Mass transfer from the Alps to the Apennines: volumetric constraints in the provenance study of the Macigno–Modino source–basin system, Chattian–Aquitanian, northwestern Italy. Sediment. Geol. 124 (1), 69–80.
Di Giulio, A., Carrapa, B., Fantoni, R., Gorla, L., Valdisturlo, L., 2001. Middle eocene to early miocene sedimentary evolution of the western segment of the south Alpine foredeep (Italy). Int. J. Earth Sci. 90, 534–548.
Dietrich, V., 1970. Die Stratigraphie der Piatta Decke. Eclogae Geol. Helv. 63, 631–671.
Doglioni, C., Harabaglia, P., Merlini, S., Mongelli, F., Peccerillo, A., Piromallo, C., 1999. Orogens and slabs vs their direction of subduction. Earth-Sci. Rev. 45, 167–208.
Dürr, S.B., 1992. Structural history of the Arosa Zone between Piatta and Err Nappes east of Marmorera (Grisons): multi-phase deformation at the Penninic-Austroalpine Plate boundary. Eclogae Geol. Helv. 85, 361–374.
Dürr, S.B., Ring, U., Frisch, W., 1993. Geochemistry and geodynamic significance of North Penninic ophiolites from the Central Alps. Schweiz. Mineral. Petrogr. Mitt. 73, 407–419.
Eiermann, D., 1988. Zur Stellung des Martegnas-Zuges. Eclogae Geol. Helv. 81, 259–272.
Engi, M., Bousquet, R., Berger, A., 2004. Explanatory notes to the map: metamorphic structure of the Alps: Central Alps. Mitt. Österr. Geol. Ges. 149, 157–173.
Favaro, S., Schuster, R., Handy, M.R., Scharf, A., Pestal, G., 2015. Transition from orogen-perpendicular to orogen-parallel exhumation and cooling during crustal indentation—key constraints from $^{147}Sm/^{144}Nd$ and $^{87}Rb/^{87}Sr$ geochronology (Tauern Window, Alps). Tectonophysics 665, 1–16.
Ferreiro Mählmann, R., Giger, M., 2010. The Arosa zone in Eastern Switzerland: oceanic, sedimentary burial, accretional and orogenic very low- to low grade patterns in a tectono-metamorphic mélange. Swiss J. Geosci. 105, 203–233.
Ferreiro-Mählmann, R., 1996. Das Diagenese-Metamorphose-Muster von Vitrinitreflexion und Illit-"Kristallinität" in Mittelbünden und im Oberhalbstein. Teil 2: Korrelation kohlenpetrographischer und mineralogischer Parameter. Schweiz. Mineral. Petrogr. Mitt. 75, 85–122.
Freeman, S.R., Butler, R.W.H., Cliff, R.a., Rex, D.C., 1998. Direct dating of mylonite evolution: a multi-disciplinary geochronological study from the Moine Thrust Zone, NW Scotland. J. Geol. Soc. 155, 745–758. https://doi.org/10.1144/gsjgs.155.5.0745.
Frisch, W., 1979. Tectonic progradation and plate tectonic evolution of the Alps. Tectonophysics 60, 121–139. https://doi.org/10.1016/0040-1951(79)90155-0.
Frisch, W., Ring, U., Dürr, S., Borchert, S., Biehler, D., 1994. The Arosa zone and Platta nappe ophiolithes (Eastern Swiss Alps): geochemical characteristics and their meaning for the evolution of the Penninic Ocean. Jb. Geol. Bundesanst. 137, 19–33.
Froitzheim, N., Schmid, S.M., Frey, M., 1996. Mesozoic paleogeography and the timing of eclogite facies metamorphism in the Alps: a working hypothesis. Eclogae Geol. Helv. 89, 81.
Gansser, A.F., 1937. Der Nordrand der Tambodecke. Schweiz. Mineral. Petrogr. Mitt. 17, 291–522.
Garzanti, E., Malusà, M.G., 2008. The Oligocene Alps: domal unroofing and drainage development during early orogenic growth. Earth Planet. Sci. Lett. 268, 487–500. https://doi.org/10.1016/j.epsl.2008.01.039.
Gebauer, D., 1996. A P-T-t path for an (ultra?) High-pressure ultramafic/mafic rock association and its felsic country rocks based on SHRIMP-dating of magmatic and metamorphic Zircon domains. Example: Alpe Arami (Central Alps). In: Earth Processes: Reading the Isotopic Code. Geophys. Monogr. 95, 307–329.
Gebauer, D., 1999. Alpine geochronology of the Central and Western Alps: new constraints for a complex geodynamic evolution. Schweiz. Mineral. Petrogr. Mitt. 79, 191–208.
Gebauer, D., Grünenfelder, M., Tilton, M., Trommsdorff, V., Schmid, S.M., 1992. The geodynamic evdution of the garnet-peridotites, garnetpyroxenites and eclogites of Alpe Arami and Cima di Gagnone (Central Alps) from Early Proterozoic to Oligocene. Eingereicht bei Schweiz. Mineral. Petrogr. Mitt. 72, 107–111.
Gerya, T.V., Stöckhert, B., Perchuk, A.L., 2002. Exhumation of high-pressure metamorphic rocks in a subduction channel: a numerical simulation. Tectonics 21, TC1056. https://doi.org/10.1029/2002TC001406.
Glodny, J., Ring, U., Kühn, A., Gleissner, P., Franz, G., 2005. Crystallization and very rapid exhumation of the youngest Alpine eclogites (Tauern Window, Eastern Alps) from Rb/Sr mineral assemblage analysis. Contrib. Mineral. Petrol. 149, 699–712. https://doi.org/10.1007/s00410-005-0676-5.
Glodny, J., Ring, U., Kühn, A., 2008a. High-pressure metamorphism, thrusting, strike-slip and extensional shearing in the Tauern Window, Eastern Alps: all starting at the same time? Tectonics 27, TC4004. https://doi.org/10.1029/2007TC002193.
Glodny, J., Kühn, A., Austrheim, H., 2008b. Geochronology of fluid-induced eclogite and amphibolite facies metamorphic reactions in a subduction-collision system, Bergen Arcs, Norway. Contrib. Mineral. Petrol. 156, 27–48. https://doi.org/10.1007/s00410-007-0272-y.
Guidotti, C.V., Sassi, F.P., 1986. Classification and correlation of metamorphic facies series by means of muscovite b0 data from low-grade metapelites. Neues Jb. Mineral. Abh. 153, 363–380.
Handy, M.R., Herwegh, M., Kamber, B.S., Tietz, R., Villa, I.M., 1996. Geochronologic, petrologic and kinematic constraints on the evolution of the Err-Platta boundary, part of a fossil continent-ocean suture in the Alps (Eastern Switzerland). Schweiz. Mineral. Petrogr. Mitt. 76, 453–474.
Heinrich, C.A., 1986. Eclogite facies regional metamorphism of hydrous mafic rocks in the Central Alpine Adula nappe. J. Petrol. 27, 123–154.
Heitzmann, P., 1975. Zur Metamorphose und Tektonik im südöstlichen Teil der Lepontin-ischen Alpen (Prov. Como, Italia). Schweiz. Mineral. Petrogr. Mitt. 55, 467–522.
Hermann, J., Müntener, O., 1992. Strukturelle Entwicklung im Grenzbereich Zwischen dem Penninischen Malenco-Ultramafitit und dem Unterostalpin (Margna- und Sella-Decke). Schweiz. Mineral. Petrogr. Mitt. 72, 225–240.
Hermann, J., Rubatto, D., Trommsdorff, V., 2006. Sub-solidus Oligocene zircon formation in garnet peridotite during fast decompression and fluid infiltration (Duria, Central Alps). Mineral. Petrol. 88, 181–206. https://doi.org/10.1007/s00710-006-0155-3.
Herwartz, D., Nagel, T.J., Münker, C., Scherer, E.E., Froitzheim, N., 2011. Tracing two orogenic cycles in one eclogite sample by Lu-Hf garnet chronometry. Nat. Geosci. 4, 178–183.
Hesse, R., 1981. The significance of synchronous versus diachronous flysch successions and distribution of arc volcanism in the Alpine-Carpathian arc. Eclogae Geol. Helv. 72, 379–381.
Hunziker, J.C., 1986. The evolution of illite to muscovite: an example of the behavior of isotopes in low-grade metamorphic terrains. Chem. Geol. 57, 31–40.
Hunziker, J.C., Desmond, J., Hurford, A.J., 1992. Thirty-two years of geochronological work in the Central and Western Alps: a review on seven maps. Mem. Geol. Lausanne 13, 1–59.
Hurford, A.J., Flisch, M., Jäger, E., 1989. Unraveling the thermo-tectonic evolution of the Alps: a contribution from fission track analysis and mica dating. Geol. Soc. Lond., Spec. Publ. 45, 369–398.
Inger, S., Cliff, R.A., 1994. Timing of metamorphism in the Tauern Window, Eastern Alps: Rb-Sr ages and fabric formation. J. Metamorph. Geol. 12, 695–707. https://doi.org/10.1111/j.1525-1314.1994.tb00052.x.
Ioannidi, I., Angiboust, S., Oncken, O., Glodny, J., Argard, P., Sudo, M., 2020. Deformation along the roof of a fossil subduction interface: the Austroalpine case and new insights from the Malenco Massif (Central Alps). Geosphere 16. https://doi.org/10.1130/GES02149.1.
Irouschek, A., 1983. Mineralogie und Petrographievon Metapeliten der Simano-Decke mit besondererBerücksichtigung cordieritführender Gesteinezwischen Alpe Sponda und Biasca. Unpubl. Ph.D.Thesis. University of Basel.
Janots, E., Engi, M., Rubatto, D., Berger, A., Gregory, C., Rahn, M., 2009. Metamorphic rates in collisional orogeny from in situ allanite and monazite dating. Geology 37, 11–14.
Jenny, H., Frischknecht, G., Kopp, J., 1923. Geologie der Adula. Beitr. Geol. Karte Schweiz NF 51.
Kassem, O.K., Ring, U., 2004. Underplating-related finite-strain patterns in the Gran Paradiso massif, Italian Western Alps: heterogeneous ductile strain superimposed on a nappe stack. J. Geol. Soc. Lond. 161, 875–884.
Kirschner, D.L., Cosca, M.A., Masson, N., Hunziker, J.C., 1996. Staircase $^{40}Ar/^{39}Ar$ spectra of fine-grained white mica; timing and duration of deformation and empirical constraints on argon diffusion. Geology 24, 747–750.
Laubscher, H.P., 1983. Detachment, shear, and compression in the Central Alps. Geol. Soc. Am. Memoir 158, 191–211.
Laubscher, H.P., 1988. The arcs of the Western Alps and the Northern Apennines: an updated view. Tectonophysics 146, 67–78.

Liati, A., Gebauer, D., 2003. Geochronological constraints for the time of metamorphism inthe Gruf complex (Central Alps) and implications for the Adula-Cima Lunga nappesystem. Schweiz. Mineral. Petrogr. Mitt. 83, 159–172.
Liati, A., Gebauer, D., Fanning, M., 2000. U-Pb SHRIMP dating of zircon from the Novate granite (Bergell, Central Alps): evidence for Oligocene-Miocene magmatism, Jurassic/cretaceous continental rifting and opening of the Valais trough. Schweiz. Mineral. Petrogr. Mitt. 80, 305–316.
Liniger, M.H., 1992. Der ostalpin-penninische Grenzbereich im Gebiet der nördlichen Margna-Decke (Graubünden, Schweiz), unpublished PhD dissertation. Eidgenössische Technische Hochschule, Zürich, p. 217. Diss. ETH Nr. 9769.
Löw, S., 1987. Die tektonometamorphe Entwicklung der nördlichen Adula-Decke. Beitr geol Karte Schweiz. Neue Folge 16, I–61.
Ludwig, K.R., 2009. Isoplot/Ex Ver 3.71: A Geochronological Toolkit for Microsoft Excel. Berkeley Geochronology Center Special Publication, Berkeley.
Malusà, M.G., Villa, I.M., Vezzoli, G., Garzanti, E., 2011. Detrital geochronology of unroofing magmatic complexes and the slow erosion of Oligocene volcanoes in the Alps. Earth Planet. Sci. Lett. 301, 324–336.
Malusà, M.G., Faccenna, C., Baldwin, S.L., Fitzgerald, P.G., Rossetti, F., Balestrieri, M.L., Danisık, M., Ellero, A., Ottria, G., Piromallo, C., 2015. Contrasting styles of (U)HP rock exhumation along the Cenozoic Adria-Europe plate boundary (Western Alps, Calabria, Corsica). Geochem. Geophys.Geosyst. 16, 1786–1824. https://doi.org/10.1002/2015GC005767.
Mancktelow, N.S., 1990. The Simplon Fault Zone. Beitr. Geol. Karte CH 163 (N.F.), p. 74.
Marquer, D., Challandes, N., Baudin, T., 1996. Shear zone patterns and strain distribution at the scale of a Penninic nappe: the Suretta nappe (Eastern Swiss Alps). J. Struct. Geol. 18, 753–764.
Massonne, H.J., Schreyer, W., 1987. Phengite geobarometry based on the limiting assemblage with K-feldspar, phlogopite, and quartz. Contrib. Mineral. Petrol. 96 (2), 212–224.
Merle, O., Guillier, B., 1989. The building of the Central Swiss Alps: an experimental approach. Tectonophysics 165, 41–56.
Meyre, C., Marquer, D., Schmid, S.M., Ciancaleoni, L., 1998. Syn-orogenic extension along the Forcola fault: Correlation of Alpine deformations in the Tambo and Adula nappes (Eastern Penninic Alps). Eclogae Geol. Helv. 91, 409–420.
Meyre, C., De Capitani, C., Zack, T., Frey, M., 1999. Petrology of high-pressure metapelites from the Adula nappe (Central Alps, Switzerland). J. Petrol. 40, 199–213.
Mohn, G., Manatschal, G., Masini, E., Müntener, O., 2011. Rift-related inheritance in orogens: a case study from the Austroalpine nappes in Central Alps (SE-Switzerland and N-Italy). Int. J. Earth Sci. 100, 937–961. https://doi.org/10.1007/s00531-010-0630-2.
Montemagni, C., Carosi, R., Fusi, N., Iaccarino, S., Montomoli, C., Villa, I.M., Zanchetta, S., 2020. Three-dimensional vorticity and time-constrained evolution of the Main Central Thrust zone, Garhwal Himalaya (NW India). Terra Nova 32. https://doi.org/10.1111/ter.12450.
Müller, W., Dallmeyer, R.D., Neubauer, F., Thöni, M., 1999. Deformation-induced resetting of Rb/Sr and $^{40}Ar/^{39}Ar$ mineral systems in a low-grade, polymetamorphic terrane (Eastern Alps, Austria). J. Geol. Soc. London 156, 261–278.
Nabholz, W., 1945. Geologie der Bündnerschiefer zwischen Rheinwald, Valser- und Safiental. Eclogae Geol. Helv. 38, 1–119.
Nänny, P., 1946. Neuere Untersuchungen im Pratigauflysch. Eclogae Geol. Helv. 39/1, 115–132.
Nänny, P., 1948. Zur geologie der Prättigauschiefer zwischen Rhättikon und Plessur. In: Gebr. Fretz A.G., Zürich, Switzerland, p. 128, 3 plates.
Nicollet, C., Bosse, V., Spalla, M.I., Schiavi, F., 2018. Eocene ultra-high temperature (UHT)metamorphism in the Gruf complex (Central Alps): constraints by LA-ICPMS zirconand monazite dating in petrographic context. J. Geol. Soc. Lond. 175, 774–787.
Nievergelt, P., Liniger, M., Froitzheim, N., Mahlmann, R.F., 1996. Early to mid Tertiary crustal extension in the Central Alps: the Turba Mylonite Zone (Eastern Switzerland). Tectonics 15 (2), 329–340.
Nitsch, K.-H., 1970. Experimentelle Bestimmungen der oberen Stabilitätsgrenze von Stilpnomelan. Fortschr. Mineral. 47, 48–49.
Oberhänsli, R., 1994. Subducted and obducted ophiolites of the Central Alps: paleotectonic implications deducted by their distribution and metamorphism overprint. Lithos 33, 109–118.
Oberhänsli, R., Goffé, B., Bousquet, R., 1995. Record of a HP-LT metamorphic evolution in the Valais zone: geodynamic implications. In: Lombardo, B. (Ed.), Studies on Metamorphic Rocks and Minerals of the Western Alps. A Volume in Memory of Ugo Pognante. Bollettino del Museo Regionale di Scienze Naturali (suppl.), Torino, pp. 221–239.
Oberli, F., Meier, M., Berger, A., Rosenberg, C.L., Gieré, R., 2004. U–Th–Pb and $^{230}Th/^{238}U$ disequilibrium isotope systematics: precise accessory mineral chronology and melt evolution tracing in the Alpine Bergell intrusion. Geochim. Cosmochim. Acta 68, 2543–2560.
Pellegrino, L., Malasina, N., Zanchetta, S., Langone, A., Tumiati, S., 2020. High pressure melting of eclogites and metasomatism of garnet peridotites from Monte Duria Area (Central Alps, N Italy): a proxy for melt-rock reaction during subduction. Lithos 358–359. https://doi.org/10.1016/j.lithos.2020.105391.
Picazo, S.M., Ewing, T., Müntener, O., 2019. Paleocene metamorphism along the Pennine–Austroalpine suture constrained by U–Pb dating of titanite and rutile (Malenco, Alps). Swiss J. Geosci. 112, 517–542.
Platt, J.P., 1986. Dynamics of orogenic wedges and the uplift of high-pressure metamorphic rocks. Geol. Soc. Am. Bull. 97, 1037–1053.
Platt, J.P., Behr, W.M., 2011. Grainsize evolution in ductile shear zones: Implications for strain localization and the strength of the lithosphere. J. Struct. Geol. 33, 537–550.
Platt, J.P., Behrmann, J.H., Cunningham, P.C., et al., 1989. Kinematics of the Alpine arc and the motion history of Adria. Nature 337, 158–161.
Pleuger, J., Hundenborn, R., Kremer, K., Babinka, S., Kurz, W., Jansen, E., Froitzheim, N., 2003. Structural evolution of the Adula nappe, Misox zone, and Tambo nappe in the San Bernardino area: constraints for the exhumation of the Adula eclogites. Mitt. Österr. Geol. Ges. 94, 99–122.
Price, J.B., Wernicke, B.P., Cosca, M.A., Farley, K.A., 2018. Thermochronometry across the Austroalpine-Pennine boundary, Central Alps, Switzerland: Orogen-Perpendicular Normal Fault Slip on a Major “Overthrust” and its implications for orogenesis. Tectonics 37, 724–757. https://doi.org/10.1002/2017TC004619.
Probst, P., 1980. Die Bündnerschiefer des nördlichen Penninikums zwischen Valsertal und Passo Giacomo. Beitr. Geol. Karte Schweiz NF 153, 64.
Ratschbacher, L., 1986. Kinematics of Austro-Alpine cover nappes: changing translation path due to transpression. Tectonophysics 125, 335–356.
Ratschbacher, L., Frisch, W., Linzer, H.-G., Merle, O., 1991. Lateral extrusion in the Eastern Alps; part 2, Structural analysis. Tectonics 10, 257–271.
Reddy, S.M., Wheeler, J., Cliff, R.A., 1999. The geometry and timing of orogenic extension: an example from the Western Italian Alps. J. Metamorph. Geol. 17, 573–589.
Ring, U., 1992a. The Alpine geodynamic evolution of Penninic nappes in the eastern Central Alps: geothermobarometric and kinematic data. J. Metamorph. Geol. 10, 33–53.
Ring, U., 1992b. The Kinematic history of the Penninic Nappes east of the Lepontine Dome: Implications for the Tectonic Evolution of the Central Alps. Tectonics 11, 1139–1158.
Ring, U., 1994a. The early Alpine orogeny in the Central Alps: a discussion of existing data. Jahrbuch Geologische Bundesanstalt Wien 137, 345–363.
Ring, U., 1994b. The kinematics of the late Alpine Muretto fault and its relation to eastward extension and to displacement at the Engadine and Periadriatic lines. Eclogae Geol. Helv. 87, 811–831.
Ring, U., Gerdes, A., 2016. Kinematics of the Alpenrhein-Bodensee graben system in the Alps: Tertiary extension due to the formation of the Western Alps arc. Tectonics 35, 1367–1391. https://doi.org/10.1002/2015TC004085.
Ring, U., Glodny, J., 2010. No need for lithospheric extension for exhuming (U)HP rocks by normal faulting. J. Geol. Soc. Lond. 167, 225–228. https://doi.org/10.1144/0016-76492009-134.
Ring, U., Kassem, O.K.K., 2007. The nappe rule: why does it work? J. Geol. Soc. Lond. 164, 1109–1112. https://doi.org/10.1144/0016-76492007-020.
Ring, U., Ratschbacher, L., Frisch, W., 1988. Plate-boundary kinematics in the Alps: motion in the Arosa suture zone. Geology 16, 696–698.
Ring, U., Ratschbacher, L., Frisch, W., Biehler, D., Kralik, M., 1989. Kinematics of the Alpine plate-margin: Structural styles, strain and motion along the Penninic–Austroalpine boundary in the Swiss–Austrian Alps. J. Geol. Soc. 146, 835–849.
Ring, U., Ratschbacher, L., Frisch, W., Dürr, S., Borchert, S., 1990. The internal structure of the Arosa Zone (Swiss–Austrian Alps). Geol. Rundsch. 79, 725–739.
Ring, U., Brandon, M.T., Willett, S., Lister, G.S., 1999. Exhumation processes. In: Ring, U., Brandon, M.T., Lister, G.S., Willett, S. (Eds.), Exhumation Processes: Normal Faulting, Ductile Flow and Erosion, 154. Geological Society London Special Publications, pp. 1–28.
Ring, U., Pantazides, H., Skelton, A., Glodny, J., 2020. Forced return flow deep in the subduction channel, Syros, Greece. Tectonics 39, 2019TC005768. https://doi.org/10.1029/2019TC005768.
Rosenberg, C., Kissling, E., 2013. Three-dimensional insight into Central-Alpine collision: lower-plate or upper-plate indentation? Geology 41, 1219–1222.
Ring, U., Yngwe, F., 2018. To be, or not to be, that is the question”—The Cretan extensional detachment, Greece. Tectonics 37, 3069–3084. https://doi.org/10.1029/2018TC005179.
Rosenberg, C.L., Berger, A., Schmid, S.M., 1995. Observations from the floor of a granitoid pluton: inferences on the driving force of final emplacement. Geology 23, 443–446.
Rubatto, D., Hermann, J., Berger, A., Engi, M., 2009. Protracted fluid-induced melting during Barrovian metamorphism in the Central Alps. Contrib. Mineral. Petrol. 158, 703–722.
Rütti, R., 2003. The Tectono-Metamorphic Evolution of the Northwestern Simano Nappe (Central Alps, Switzerland). Unpubl. PhD Thesis no. 15149. ETH Zürich, p. 111.
Rütti, R., Marquer, D., Thompson, A.B., 2008. Tertiary tectono-metamorphic evolution of the European margin during Alpine collision: example of the Leventina Nappe (Central Alps, Switzerland). Swiss J. Geosci. 101 (Supplement 1), S157–S171. https://doi.org/10.1007/s00015-008-1278-9.
Scheiber, T., Pfiffner, O.A., Schreurs, G., 2012. Strain accumulation during basal accretion in continental collision: a case study from the Suretta Nappe (Eastern Swiss Alps). Tectonophysics 579, 56–73. https://doi.org/10.1016/j.tecto.2012.03.009.
Schmid, S.M., Froitzheim, N., 1993. Oblique slip and block rotation along the Engadine line. Eclogae Geol. Helv. 86, 569–593.
Schmid, S.M., Hass, R., 1989. Transition from near-surface thrusting to intra-basement decollement; Schlinig thrust; eastern Alps. Tectonics 8, 697–718.
Schmid, S., Rück, Ph., Schreurs, G., 1990. The significance of the Schams nappes for the reconstruction of the paleotectonic and orogenic evolution of the Penninic zone along the NFP-20 east traverse (Grisons, eastern Switzerland). In: Roure, R., Heitzmann, P., Polino, R. (Eds.), Deep structure of the Alps, 156. Mem. Soc. geol. Fr, Paris, pp. 263–287.
Schmid, S.M., Pfiffner, O.A., Froitzheim, N., Schönborn, G., Kissling, E., 1996. Geophysical-geological transect and tectonic evolution of the Swiss-Italian Alps. Tectonics 15, 1036–1064. https://doi.org/10.1029/96TC00433.

Schmid, S.M., Fügenschuh, B., Kissling, E., Schuster, R., 2004. Tectonic map and overall architecture of the Alpine orogen. Eclogae Geol. Helv. 97, 93–117.
Schreurs, G., 1993. Structural analysis of the Schams nappes and adjacent tectonic units: implications for the orogenic evolution of the Penninic Zone in eastern Switzerland. Bull. Soc. Géol. France 164, 415–435.
Schuster, R., Scharbert, S., Abart, R., Frank, W., 2001. Permo-Triassic extension and related HT/LP metamorphism in the Austroalpine - Southalpine realm. Mitt. Ges. Geol. Bergbaustud. Österr. 45, 111–141.
Schuster, R., Koller, F., Hoeck, V., Hoinkes, G., Bosquet, R., 2004. Explanatory notes to the map of the Alps: metamorphic structure of the Alps. Metamorphic evolution of the eastern Alps. Mittt. Österr. Min. Ges. 149, 71–95.
Seidlitz, von, 1906. Geologische Untersuchungen im Östlichen Rätikon. Ber. Naturf. Ges. Freiburg i.B. 16, 232–366.
Simon-Labric, T., Rolland, Y., Dumont, T., Heymes, T., Authermayou, C., Corsini, M., Fornari, M., 2009. $^{40}Ar/^{39}Ar$ dating of Penninic Front tectonic displacement (W Alps) during the lower Oligocene (31–34 Ma). Terra Nova 21, 127–136.
Spicher, A., 1980. Tectonic map of Switzerland 1:5000,000. In: Atlas der Schweiz. Bundesamt für Landestopographie, Wabern.
Staub, R., 1926. Geologische Karte des Avers. Beitr. Geol. Karte Schweiz NF 97.
Steck, A., 1984. Structures et déformations tertiaires dans les Alpes centrales. Eclogae Geol. Helv. 77, 55–100.
Steck, A., Hunziker, J., 1994. The Tertiary structural and thermal evolution of the Central Alps - compressional and extensional structures in an orogenic belt. Tectonophysics 238, 229–254.
Steinitz, G., Jäger, E., 1981. Rb-Sr and K-Ar studies on rocks from the Suretta nappe, Eastern Switzerland. Schweiz. Mineral. Petrogr. Mitt. 61, 121–131.
Steinmann, M., 1994. Ein Beckenmodell für das Nordpenninikum der Ostschweiz. Jahrb. Geol. Bundesanst. 137, 675–721.
Steinmann, M., Stille, P., 1999. Geochemical evidence for the nature of the crust beneath the eastern North Penninic basin of the Mesozoic Tethys Ocean. Geol. Rundsch. 87, 633–643.
Strobach, H., 1965. Der mittlere Abschnitt der Tambodecke samst seiner mesozoischen Unterlage und Bedeckung. Mitt. geol. Inst. ETH u. Univ. Zurich, [N.F.] 38.
Trommsdorff, V., 1983. Petrologic aspects of serpentinite metamorphism. Rendiconti Soc. Ital. Mineral. e Petrol. 38 (2), 549–559.
Trommsdorff, V., Evans, B.W., 1974. Alpine Metamorphism of Peridotitic Rocks. Schweiz. Mineral. Petrogr. Mitt. 54, 333–352.
Trümpy, R., 1960. Paleotectonic evolution of the Central and Western Alps. Geol. Soc. Am. Bull. 71, 843–907.
Trümpy, R., 1980. Geology of Switzerland: An Outline of the Geology of Switzerland. Schweiz. Geol. Komiss, Wepf (Basel), p. 104.
Tumiati, S., Zanchetta, S., Pellegrino, L., Ferrario, C., Casartelli, S., Malaspina, N., 2018. Granulite-facies overprint in garnet peridotites and kyanite eclogites of MonteDuria (Central Alps, Italy): clues from srilankite- and sapphirine-bearingsymplectites. J. Petrol. 59, 115–152.
Villa, I.M., 2010. Disequilibrium textures versus equilibrium modelling: geochronology at the crossroads. Geol. Soc. Lond., Spec. Publ. 332 (1), 1–15.
Villa, I.M., 2016. Diffusion in mineral geochronometers: present and absent. Chem. Geol. 420, 1–10.
Villa, I.M., De Bièvre, P., Holden, N.E., Renne, P.R., 2015. IUPAC-IUGS recommendation on the half life of $^{87}Rb$. Geochim. Cosmochim. Acta 164, 382–385. https://doi.org/10.1016/j.gca.2015.05.025.
Villa, I.M., Hermann, J., Müntener, O., Trommsdorff, V., 2000. $^{39}Ar$-$^{40}Ar$ dating of multiply zoned amphibole generations Paleocene metamorphism of the Pennine-Austroalpine boundary (Malenco, Italian Alps). Contrib. to Mineral. Petrol. 140, 363–381.
von Blanckenburg, F., 1992. Combined high-precision chronometry and geochemical tracing using accessory minerals: applied to the Central Alpine Bergell intrusion. Chem. Geol. 100, 19–40.
Waibel, A.F., Frisch, W., 1989. The Penninic wildflysch of the lower Engadine window, sediment deposition and accretion in relation to the plate-tectonic evolution of the Eastern Alps. Tectonophysics 162, 229–241.
Weber, W., 1966. Zur Geologie zwischen Chiavenna und Mesocco, 57. Mitt. Geol. Inst. ETH Univ, Zurich, (N.F.), p. 248.
Weh, M., 1998. Tektonische Entwicklung der penninischen Sediment-Decken in Graubünden (Prättigau bis Oberhalbstein). Unpublished PhD thesis, University of Basel, p. 230.
Weh, M., Froitzheim, N., 2001. Penninic cover nappes in the Prättigau half-window (Eastern Switzerland): structure and tectonic evolution. Eclogae Geol. Helv. 94, 237–252.
Wheeler, J., Butler, R.W.H., 1994. Criteria for identifying structures related to true crustal extension in orogens. J. Struct. Geol. 16, 1023–1027.
Wheeler, J., Reddy, S.M., Cliff, R.A., 2001. Kinematic linkage between internal zone extension and shortening in more external units in the NW Alps. J. Geol. Soc. Lond. 158, 439–443.
Wiederkehr, M., Sudo, M., Bousquet, R., Berger, A., Schmid, S.M., 2009. Alpine orogenic evolution from subduction to collisional thermal overprint: the $^{40}Ar/^{39}Ar$ age constraints from the Valaisan Ocean, Central Alps. Tectonics 28, TC6009.
Winkler, W., 1988. Mid- to early Late Cretaceous flysch and melange formations in the western part of the Eastern Alps. Paleotectonic implications. Jb. Geol. Bundes-Anstalt. 131, 341–389.
Ziegler, W.H., 1956. Geologische Studien in den Flyschgebieten des Oberhalbsteins (Graubünden). Eclogae Geol. Helv. 49, 1–81.